Underwater Vehicle Localization Using Range Measurements

by

Georgios Papadopoulos

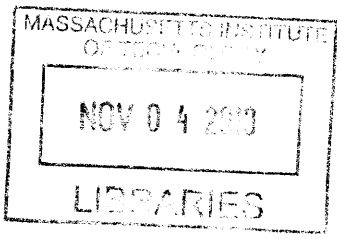

ARCHIVES

Submitted to the Department of Mechanical Engineering
in partial fulfillment of the requirements for the degree of

Master of Science

at the

MASSACHUSETTS INSTITUTE OF TECHNOLOGY

September 2010

Author .....
Department of Mechanical Engineering
August 21, 2010

Certified by .....
John J. Leonard
Professor of Mechanical and Ocean Engineering
Thesis Supervisor

Certified by .....
Nicholas M. Patrikalakis
Kawasaki Professor of Engineering
Thesis Supervisor

Accepted by .....
David E. Hardt
Chairman, Department Committee on Graduate Students
Mechanical Engineering Department

Underwater Vehicle Localization Using Range Measurements

by

Georgios Papadopoulos

Submitted to the Department of Mechanical Engineering
on August 21, 2010, in partial fulfillment of the
requirements for the degree of
Master of Science

Abstract

This thesis investigates the problem of cooperative navigation of autonomous marine vehicles using range-only acoustic measurements. We consider the use of a single maneuvering autonomous surface vehicle (ASV) to aid the navigation of one or more submerged autonomous underwater vehicles (AUVs), using acoustic range measurements combined with position measurements for the ASV when data packets are transmitted. The AUV combines the data from the surface vehicle with its proprioceptive sensor measurements to compute its trajectory. We present an experimental demonstration of this approach, using an extended Kalman filter (EKF) for state estimation.

We analyze the observability properties of the cooperative ASV/AUV localization problem and present experimental results comparing several different state estimators. Using the weak observability theorem for nonlinear systems, we demonstrate that this cooperative localization problem is best attacked using nonlinear least squares (NLS) optimization. We investigate the convergence of NLS applied to the cooperative ASV/AUV localization problem. Though we show that the localization problem is non-convex, we propose an algorithm that under certain assumptions (the accumulative dead reckoning variance is much bigger than the variance of the range measurements, and that range measurement errors are bounded) achieves convergence by choosing initial conditions that lie in convex areas. We present experimental results for this approach and compare it to alternative state estimators, demonstrating superior performance.

Thesis Supervisor: John J. Leonard
Title: Professor of Mechanical and Ocean Engineering

Thesis Supervisor: Nicholas M. Patrikalakis
Title: Kawasaki Professor of Engineering

Acknowledgments

First and foremost, I would like to thank my advisors, John Leonard and Nicholas Patrikalakis, for their continuous support and direction. They are always available to discuss ideas and have provided me with the necessary materials and guidance to successfully pursue my research topic.

I would also like to thank Maurice for working alongside me on this project and sharing his ideas and opinions. He contributed much when it came to conducting experiments and providing input. I would like to thank the members of my research group, including Jacque, Aisha, Michael, Hordur, Been, Andrew, and Rob for all the discussions they shared with me. Being able to discuss and bounce ideas off of each other is one of the most important aspects of research; it is the backbone of developing innovative ideas, and I have been very fortunate to have been able to work with such excellent, fruitful minds.

In addition, I would like to thank my family for the support that they have provided me during the course of my undergraduate and graduate studies. Lastly, I would like to thank my friends at MIT for their support, including: Sertac, Gleb, Kathy, Alex, Tracey, and James.

The research described in this thesis was funded in part by the Singapore National Research Foundation (NRF) through the Singapore-MIT Alliance for Research and Technology (SMART) Center for Environmental Sensing and Modeling (CENSAM) and by the Office of Naval Research.

THIS PAGE INTENTIONALLY LEFT BLANK

Contents

List of Figures

THIS PAGE INTENTIONALLY LEFT BLANK

List of Tables

THIS PAGE INTENTIONALLY LEFT BLANK

Chapter 1

Introduction

This thesis investigates the problem of cooperative navigation of autonomous marine vehicles using range-only acoustic measurements. We consider the use of a single maneuvering autonomous surface vehicle (ASV) to aid the navigation of one or more submerged autonomous underwater vehicles (AUVs), using acoustic range measurements combined with position measurements for the ASV when data packets are transmitted. In this chapter we provide a brief review of the previous literature on AUV navigation cooperative localization, and then provide an overview of the structure of the remainder of the thesis.

1.1 AUV Navigation

AUVs are important in many marine applications, such as ocean mapping and exploration, ship inspection and environmental research. Accurate AUV localization is an important enabler for AUV navigation and autonomy. There are many different approaches to AUV navigation, including the use of inertial/Doppler velocity log systems [41], acoustic transponders [17, 21], and simultaneous localization and mapping (SLAM) techniques [29, 12].

While many terrestrial robots navigate using the Global Positioning System (GPS), this solution is not available underwater due to the fact that electromagnetic energy cannot propagate appreciable distances in the water. Of course, many AUVs surface

to obtain GPS fixes, but this is undesirable for many missions. Thus, a key requirement for many AUV tasks is to achieve a bounded error without reliance on surfacing for GPS measurements.

Knowledge of an underwater vehicle's position can be obtained by dead-reckoning (DR), using an Inertial Navigation System (INS) and a Doppler Velocity Log (DVL) [41]. The vehicle's position is computed or propagated by incorporating the velocity measurements with the vehicle's heading measurements from a magnetic compass. For example, see Hegrenas *et al.* [18] for recent paper that combines DVL measurements and with a model of the vehicle's dynamics in a Kalman filter framework to improve position estimation.

Regardless of sensor accuracy, the localization error grows continuously. This was the motivation for other researchers to solve the problem by using DR navigation and having the vehicle surfaces to get a GPS fix when its uncertainty is not small enough to be able to navigate and to operate. However this procedure wastes both time and energy, and incurs a risk of collision with vehicles at the surface.

Another method for AUV navigation is to employ SLAM techniques [29, 12, 37]. SLAM techniques will encounter difficulties in environments where are no feature on the seabed. In addition, the sensors used for SLAM approaches (such as forward looking sonars) can be quite expensive.

Currently, probably the most popular way of localizing an underwater vehicle is using long baseline (LBL) navigation [17, 21]. In this approach, two or more transponders (beacons) are installed on the sea bed or in the water column at known positions, indicating the operation area. When an underwater vehicle needs to navigate in this area to perform a task, it then sends an acoustic signal to alert and inform beacons that it needs to be guided to be navigated and localized. When a beacon receives a ping from an AUV, it then generates and sends a message to the vehicle with its unique beacon ID number. The position is then determined by knowing the beacon's locations and by measuring the message's travel time. Finally the relative range distances between vehicles are obtained by multiplying the message traveling time by the speed of sound in water. Estimation of the AUV position can be obtained by integrat-

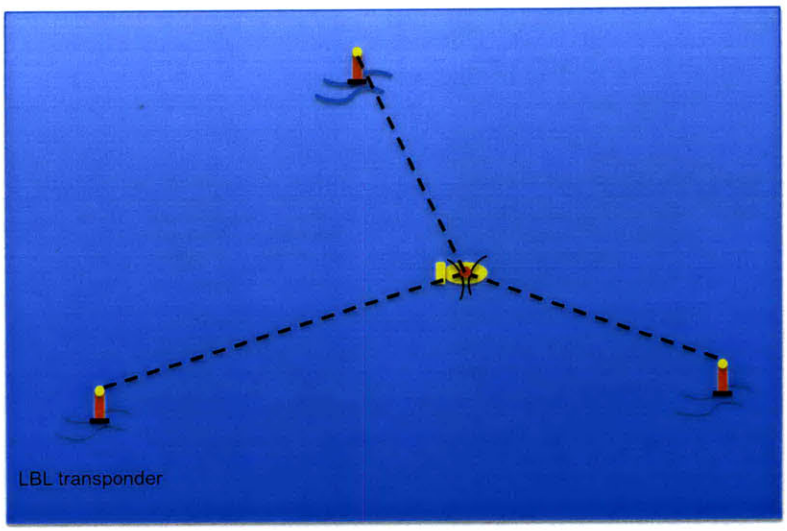

Figure 1-1: Long baseline localization.

ing all the range measurements gathered and applying them to a state estimator [40]. Through integrating these range measurements with velocity measurements from a DVL or INS, a better estimate of the vehicle's position can be obtained [19, 1].

Another variation of acoustic beacon-based navigation systems is Ultra-Short Base Line (USBL) navigation [30]. In USBL, multiple hydrophones are used to enable both the range and angle between the AUV and the beacon to be measured. Applications of USBL can be found in Mandt *et al.* [27] and Rigby *et al.*[33].

1.2 Cooperative AUV Localization

The cooperative localization of multiple AUVs has been previously investigated by quite a few researchers, including Vaganay *et al.* [36] and Bahr *et al.* [5]. In this work, multiple AUVs equipped with acoustic modems help one another to navigate by sharing position information and acoustic range measurements. The original concept, named Moving Long Baseline (MLBL), envisioned two types of AUVs: a Search-Classify-Map (SCM) vehicles, whose task was oceanographic mapping [36] and a Comm-Nav-Aid (CNA) vehicles, whose task was to aid the SCM vehicle's navigation. The system design called for the CNA vehicles to be equipped with high-performance inertial/Doppler systems, and also for the CNA vehicles to surface frequently for GPS

Figure 1-2: The autonomous kayaks we consider in this thesis: MIT SCOUT autonomous kayaks.

fixes, whereas the SCM vehicles would have low-cost proprioceptive sensors.

So as to simplify the problem at this stage, the CNA role has been taken by an autonomous surface vehicle (ASV) with continuous access to GPS. Using an acoustic modem for the ranging, the surface vehicle sends its GPS location estimate with each transmission. If the AUV receives such a message it combines the information with its own dead-reckoning within an estimation framework to improve its position estimate. The approach can either make use of round-trip acoustic ranging, or if the vehicles have synchronized clocks, using one-way acoustic travel time measurements.

Previous work on cooperative localization has relied on the use of two or more CNA vehicles, spaced sufficiently far apart to establish a wide baseline, hence the name MLBL [36]. In more recent work, we have pursued the same goal using only a single surface vehicle [13] and exploiting its motion to achieve similar performance as when two ore more CNAs are used. In this thesis we analyze the observability of this configuration for marine cooperative localization and show that a single surface vehicle can localize the AUV, if its motion is chosen appropriately.

Moving forward from the use of two surface vehicles to aid one AUV [6], in this thesis we investigate the problem of cooperative localization using a single ASV and

one or more AUVs. Our work is closely related to the work of Eustice *et al.*, who have investigated the localization of a submerged AUV using one-way acoustic travel time measurements between the AUV and a manned surface vessel [11, 39, 38]. In both approaches, GPS data and acoustic range measurements from a surface vehicle are fused onboard an AUV to compute the AUV's trajectory. Eustice and Webster's work has primarily targeted the use of higher cost AUVs for which a Doppler Velocity Log is available.

There are a number of estimation algorithms which can be used to solve this problem, including the Extended Kalman Filter (EKF), Particle Filtering (PF), and Nonlinear Least Squares (NLS) optimization methods [11]. Also modern nonlinear theories such as contraction theory [26] have motivated some researchers to investigate AUV navigation and control using nonlinear observers that take into account vehicle dynamics [25]. This approach has not yet been applied to this problem.

Cooperative AUV localization is a special category of a more general field of cooperative autonomy. The cooperative localization for ground vehicles has been extensively studied by Roumeliotis and colleagues [31], assuming reliable communications. In the AUV setting, we are encumbered by low bandwidth communications with high latency.

Gadre has provided a solution to the underwater localization problem by using range measurements from a single beacon at known fixed position [15],[16],[28]. His approach takes into account water currents. He has also provided an observability analysis of the LBL problem that we will discuss later, the observability analysis and taking into account the water currents are the main contributions of his work.

LBL and USBL systems give good position accuracy (with an accuracy on the order of several meters), however the operation area of the robots is restricted to few square kilometers (at most $10km^2$). Our goal in this work is to be able to localize an AUV (without GPS access) using noisy velocity measurements, while receiving relative range measurements from one autonomous surface vehicle (ASV) with access to GPS. The ASV travels along with the underwater vehicle, and therefore the operation of the vehicles is not restricted to a predefined area, as with LBL. The

Vehicles communicate with one another using acoustic modems [14].

1.3 Outline of the Thesis

The structure of the thesis is as follow. Chapter 2 defines the cooperative localization problem, providing an observability analysis that shows that a non-linear observer is better suited than linear techniques for this problem. Chapter 3 reviews several recursive state estimation approaches that previous researchers have used to address this problem. Motivated from the observability analysis presented in the Chapter 2, in Chapter 4, we propose a solution to the MLBL problem using NLS. A convergence analysis for this algorithm is provided. In Chapter 5, we present the experimental results for the thesis, comparing the different state estimators that we investigated. Finally, Chapter 6 concludes the thesis by summarizing our contributions and making suggestions for future research.

Chapter 2

Cooperative ASV/AUV Localization Problem Using a Single Surface Vehicle

This chapter defines the cooperative localization problem. We begin by providing a mathematical description of the cooperative ASV/AUV localization problem. More specifically we give the equations of motion for an underwater vehicle, and will describe the measurements taken to help the vehicle localize itself. We see that without relative measurements from a known position, the system covariance increases continuously without bound. Subsequently, we provide an observability analysis of the system. We prove that if the vehicle obtains range measurements from a known position, the system will be observable, and therefore an observer can be applied to solve the problem. Finally, we study the problem of choosing the ASV's trajectory to reduce system uncertainty in each direction.

2.1 Problem Definition

In marine robotics, the cooperative ASV/AUV localization problem has been developed as follows [13]: acoustic modems are installed on one or more surface vehicles and one or more AUVs. The surface vehicle moves in formation with the AUV

and continuously broadcasts messages that contain its GPS location and associated timestamp. If the AUV receives one of these messages, and assuming synchronous timing on each vehicle [10], the range between the two vehicles can be computed. The AUV then combines this information with its own dead-reckoning filter, in a Bayesian framework, to estimate its position.

The AUV is equipped with sensors that can measure its velocity in the forward, $\hat{v}_m$, and starboard directions, $\hat{w}_m$, and a compass that measures its absolute heading, $\hat{\theta}_m$ at each time increment, m. A pressure sensor measures the vehicle depth precisely, which allows the 3-D problem to be simplified to 2-D. The vehicle position $X_1 = [x_1 \; y_1]^T$ is propagated by the equations below.

$$\begin{aligned} x_{1,[m+1]} &= x_{1,[m]} + \triangle_m(\hat{v}_m \cos\hat{\theta}_m - \hat{w}_m \sin\hat{\theta}_m) \\ y_{1,[m+1]} &= y_{1,[m]} + \triangle_m(\hat{v}_m \sin\hat{\theta}_m + \hat{w}_m \cos\hat{\theta}_m) \end{aligned} \tag{2.1}$$

This propagation will operate with a frequency of 5Hz, thus $\triangle_m = 0.2$ sec.

The expectation of a random variable x_1 is defined as its average value over a large number of experiments (μ_{x_1} or $E[x_1]$). In the estimation problem, to know the mean of a random variable is not enough; we also need to know its variance and minimize it. The variance of a random variable is given by:

$$Var(x_1) = \sigma_{x_1}^2 = E[(x_1 - \mu_{x_1})^2] = E[x_1^2] - (\mu_{x_1})^2 \tag{2.2}$$

In our case we have a vector of two random variables $X_1 = [x_1 \; y_1]^T$; then we can define the covariance matrix as:

$$P_{X_1} = E[(X - \mu_{x_1})(X - \mu_{x_1})^T] \tag{2.3}$$

The velocity measurements are considered to be observations of a combination of a deterministic value and a stochastic part with zero mean Gaussian noise ($n_{\hat{v}}$, $n_{\hat{w}}$

and $n_{\hat{\theta}}$).

$$\begin{aligned} v_m &= \hat{v}_m + n_{\hat{v}} \\ w_m &= \hat{w}_m + n_{\hat{w}} \\ \theta_m &= \hat{\theta}_m + n_{\hat{\theta}} \end{aligned} \tag{2.4}$$

Furthermore, if the vehicle heading is a deterministic variable then the analysis can be simplified. As we will show later in this work, the heading can be treated as a deterministic variable if we combine its effect with the effect of the velocity's variance.[1] In this case, the system equations are equivalent to the equations below:

$$\begin{aligned} x_{1,[m+1]} &= x_{1,[m]} + \triangle_m(\hat{v}_{eq,m}\cos\hat{\theta}_m - \hat{w}_{eq,m}\sin\hat{\theta}_m) \\ y_{1,[m+1]} &= y_{1,[m]} + \triangle_m(\hat{v}_{eq,m}\sin\hat{\theta}_m + \hat{w}_{eq,m}\cos\hat{\theta}_m) \end{aligned} \tag{2.5}$$

From the above equations we can see that the states are random variables with variance that increases continuously as the time (t) increases:

$$\begin{aligned} \sigma^2_{x_1}(t) &= \sigma^2_{t=0} + (\sigma^2_{V_{eq}}\cos^2\theta_d + \sigma^2_{W_{eq}}\sin^2\theta_d)t^2 \\ \sigma^2_{y_1}(t) &= \sigma^2_{t=0} + (\sigma^2_{V_{eq}}\cos^2\theta_d + \sigma^2_{W_{eq}}\sin^2\theta_d)t^2 \end{aligned} \tag{2.6}$$

Accordingly, as the vehicle's dead-reckoning is propagated, the localization error and uncertainty will grow. As mentioned above, a range measurement from the surface vehicle will occasionally be received (with frequency of at most 0.1Hz, thus $\triangle_i = 10$ sec) and will be used to bound this uncertainty. The surface vehicle trajectory at each such time i is denoted by $X_{2,[i]} = [x_{2,[i]}, y_{2,[i]}]^T$, and the associated range measurement by $h_{3D,[i]}$. Assuming accurate depth information, this range measurement is converted

[1] This is the case when the variance of the vehicle's heading is much smaller than the variance of the velocity sensors; we consider this a reasonable assumption when the vehicle is not equipped with a DVL or an INS system.

into a horizontal range, $h_{[i]}$. The measurement function is given by:

$$h_{[i]} = \sqrt{(x_{1,[i]} - x_{2,[i]})^2 + (y_{1,[i]} - y_{2,[i]})^2} + n_r \tag{2.7}$$

Where n_r is the range measurements noise which is consider to be zero mean Gaussian noise.

Figure 2-1 illustrates this framework. Note that the heading is not considered in the observability analysis in the next section as it is directly observable. While further details of the cooperative ASV/AUV localization problem can be found in [6, 13], in this thesis we will focus on the observability and convexity of the problem.

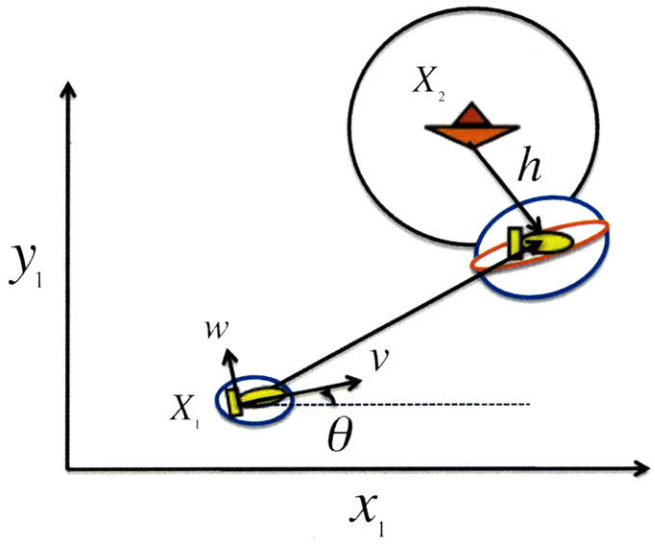

Figure 2-1: An AUV navigates using measurements of its heading, θ, and velocities, v and w, however its uncertainty grows overtime (blue circle). Occasionally a surface vehicle provides the AUV with a range measurement (black circle), information that the AUV uses to reduce its uncertainty (red).

2.2 Observability Analysis

2.2.1 Introduction

Observability is an important property of the system. If the system described in Equations 2.1 and 2.7 is observable, the vehicle's position can be observed by combining the dead-reckoning measurements with the range measurements. Observability depends on the relative motion between the two vehicles. If the system is not observable, then there is no way the vehicle's position can be computed, regardless of the estimation algorithm used.

It is important to state that the observability of a linear system does not depend on the estimator used to recover the states; however, by linearizing a non-linear system, important information maybe discarded. Therefore, one can identify cases in which the actual non-linear system is observable and at the same time the linearized system is unobservable. The cooperative ASV/AUV localization problem is one of these cases.

Some notable previous work has considered the observability of the cooperative ASV/AUV localization problem. Gadre [16] performed an observability analysis for a similar system with a stationary ranging beacon. The approach taken linearized the system leading to important information being lost in the process. Gadre asserted that an AUV receiving range measurements from known locations can recover its states if the direction from which these measurements are taken varies over time. However given that the vehicles may not be particularly mobile (due to performance or mission constraints), a non-linear method which maximizes observability at all times would be beneficial. More recently, Antonelli *et al.* [2] examined locally weak observability of the cooperative ASV/AUV localization problem, presenting results for an EKF used for cooperative localization, with simulations using two surface craft.

In both of these cases of previous research, linearization is performed, thereby assuming that the system is a linear time variant system. In doing so, important information is lost. The resulting linearized system will be unobservable if the direction

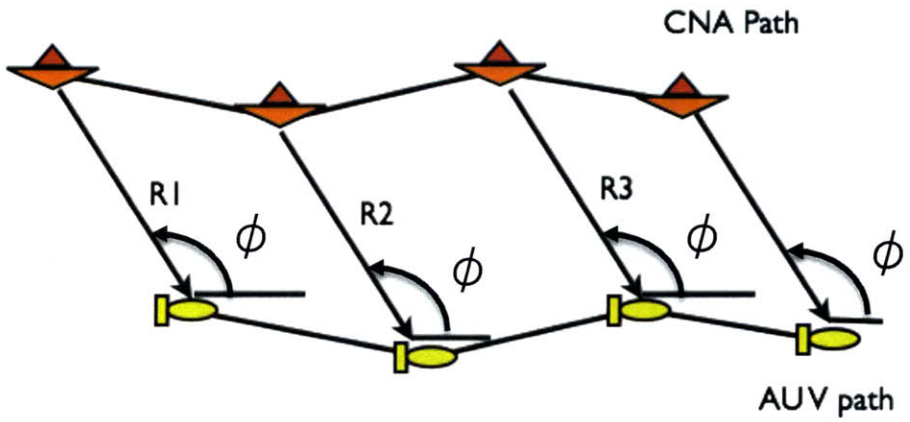

Figure 2-2: The vehicle receives range measurements that come from the same direction. In this case the linearized system is unobservable.

from which the range measurements are taken from do not vary over time, as shown in Figure 2-2.

To recover this property, consider Figure 2-3. In Figure 2-3(a) we can see the effect of linearizing a range measurement. In Figure 2-3(b) the AUV has just received one range measurement from the ASV. Subsequently, both vehicles move to new positions and the ASV provides the AUV with another measurement, however we use dead-reckoning measurements and therefore we can treat the AUV as stationary. Looking at Figure 2-3(b), we can see that if the range measurements come from different directions, then the vehicle position can be recover by solving for the intersection of the linearized ranges, and therefore the system is observable; this agrees with Gadre's results.

In Figure 2-3(c), the AUV has just received a range measurement from the ASV, and then the ASV moves to another location and provides the AUV with another range measurement from a different but co-linear location. According to Gadre's results, this system is unobservable. However, if a linearization has not been carried out, the system would be observable, as the AUV position could be computed by solving for the intersection. Note that computing this solution with might still be very challenging, as with significant measurement uncertainty the problem will be ill-conditioned; we discuss this issue in more detail below.

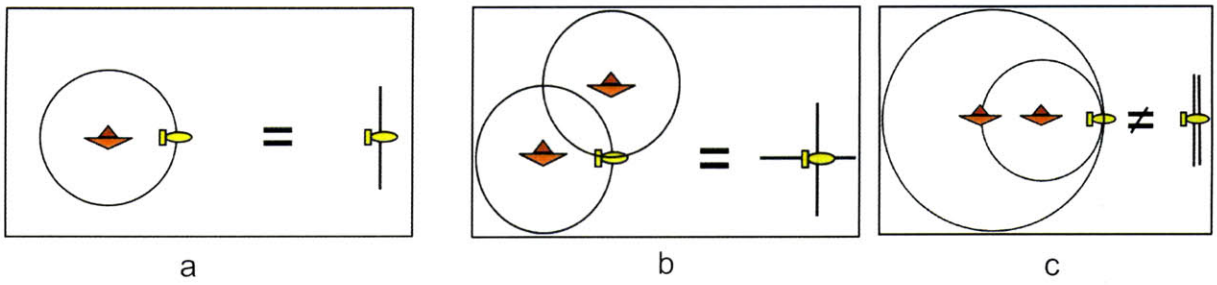

Figure 2-3: Linearization effects on the observability.

2.2.2 Observability Analysis Using the Weak Observability Theorem

The scenario that we have just discussed motivates us to study the observability of the actual non-linear system. In this section, we will use non-linear observability theory to prove that the system is locally weak observable. Again, we assume that the vehicle heading can be measured directly, and hence it will not be considered, leaving a second order system in x_1 and y_1.

For a nonlinear estimator, such as a particle filter, of a non-linear measurement function, h, one can observe the system if the gradient of the Lie derivative matrix, G, is a full rank matrix, according to the weak observability theorem [34, 20]. The observability matrix is given by

$$Obs = d(G) = \begin{pmatrix} dL_f^0(h_1) & \dots & dL_f^0(h_m) \\ dL_f^1(h_1) & \dots & dL_f^1(h_m) \\ \vdots & \ddots & \vdots \\ dL_f^{n-1}(h_1) & \dots & dL_f^{n-1}(h_m) \end{pmatrix} \tag{2.8}$$

where $L_f^{n-1}(h_m)$ is the Lie derivative of the measurement m in dimension n.

While our dynamical system is a third order system, as discussed above, we assume we have access to a direct estimate of the vehicle heading. For this reason, we will simplify the observability analysis to a second order system in x_1 and y_1, and thus

$n = 2$. The continuous system equivalent is given by:

$$\dot{X_1} = f(X_1, u) \tag{2.9}$$

where

$$f = \begin{pmatrix} f_1 \\ f_2 \end{pmatrix} = \begin{pmatrix} \hat{v}\cos\hat{\theta} + \hat{w}\sin\hat{\theta} \\ \hat{v}\sin\hat{\theta} - \hat{w}\cos\hat{\theta} \end{pmatrix} \tag{2.10}$$

For range-only measurements, with $m = 1$, the non-linear measurement function is given by

$$h = h_1 = \sqrt{(X_1 - X_2)^T(X_1 - X_2)} = \sqrt{(x_1 - x_2)^2 + (y_1 - y_2)^2} \tag{2.11}$$

the Lie derivatives are as follows

$$L_f^0(h) = h \tag{2.12}$$

$$L_f^1(h) = \begin{pmatrix} \frac{x_1 - y_2}{h} & \frac{y_1 - y_2}{h} \end{pmatrix} \begin{pmatrix} f_1 \\ f_2 \end{pmatrix} \tag{2.13}$$

which gives

$$G = \begin{pmatrix} h \\ \frac{(x_1 - x_2)f_1 + (y_1 - y_2)f_2}{h} \end{pmatrix} \tag{2.14}$$

Our specific observability matrix is formed from the derivative of G with respect to the AUV state vector X_1

$$\begin{aligned} Obs &= d(G) = d\begin{pmatrix} L_f^0(h) \\ L_f^1(h) \end{pmatrix} \\ &= \begin{pmatrix} \frac{(x_1 - x_2)}{h} & \frac{(y_1 - y_2)}{h} \\ \frac{(y_1 - y_2)^2 f_1 - (x_1 - x_2)(y_1 - y_2)f_2}{h^3} & \frac{-(x_1 - x_2)(y_1 - y_2)f_1 + (x_1 - x_2)^2 f_2}{h^3} \end{pmatrix} \end{aligned} \tag{2.15}$$

This system is observable if the observability matrix is full rank. Thus, if

$$\det(Obs) = \frac{-f_1(y_1 - y_2) + f_2(x_1 - y_2)}{h^2} \neq 0 \tag{2.16}$$

Looking at the observability matrix, we can see that it is full rank and therefore the system is always observable. Some of the trivial cases that Gadre identified the system to be unobservable, [16], now using non-linear theory, have been shown to be observable as long as the ASV-to-AUV range changes. In summary, the observability with a linear estimator is guaranteed by the relative motion between the vehicles, but can be improved upon by the use of a nonlinear estimator as well as ASV motion planning.

2.3 Surface Vehicle Trajectory

According to the above analysis the system is observable and therefore an observer can be applied to solve the problem. Even if the system is observable this does not mean that it will converge. The convergence depends on the system dynamics, the noise characteristics, frequency of the measurements and the positions that the relative measurements are taken from. Each time the vehicle receives DR measurements its uncertainty grows in each direction. In addition, each time the vehicle receives a range measurement its uncertainty reduces in only the radial direction since the other directions are unobservable directions.

The system becomes unobservable if the determinant of the observability matrix is equal to zero. There are also cases for which the system is almost unobservable. One of these cases occurs when the observability matrix is "ill-conditioned ", meaning that the range measurements are not informative enough to localize the vehicle. This can motivate us to design ASV trajectories that will maximize the condition number of the observability matrix. This can be done by running search algorithms that compute the trajectory of the ASV that maximizes the determinant of the observability matrix.

In the above analysis, we did not refer to terms like uncertainty. The analysis

above also made no assumptions on noise characteristics. Another way to analyze this problem is through uncertainty analysis. This problem was stated and solved by Zhou *et al.*, considering the Kalman filtering framework [43]. This work demonstrated that in order to minimize uncertainty in each direction, we need to provide the vehicle at each step with range measurements in the direction of the larger eigenvalue of the covariance matrix. Simple intuition agrees with this and states that all the sequential range measurements should be orthogonal to each other, since we want to gather as much information as we can in each step.

Greedy optimization algorithms can be applied to plan the surface vehicle's trajectory. A typical structure of such an algorithm has a discretization step in which the reachable space is computed for several time steps into the future. An EKF algorithm is then used to compute the covariance resulting if the surface vehicle were at one of these points. This is done for all points. Then the surface vehicle is moved to the point giving the smallest covariance. An approach of this nature can be found in [4].

To illustrate some of the benefits to be achieved by planning the ASV trajectory, we present simulation results of such an approach in Figure 2-4. In this figure, the surface vehicle's position is computed in such a way that the range measurements are to be taken from the direction of the largest eigenvalues of the covariance matrix. The covariance matrix is computed using particle filtering, giving better results than would be achieved with an EKF.

2.4 Summary

This chapter has presented a problem statement for ASV/AUV cooperative localization, and investigated the problem using nonlinear observability theory. In the next chapter, we apply two recursive state estimators — extended Kalman filtering and particle filtering — to this problem.

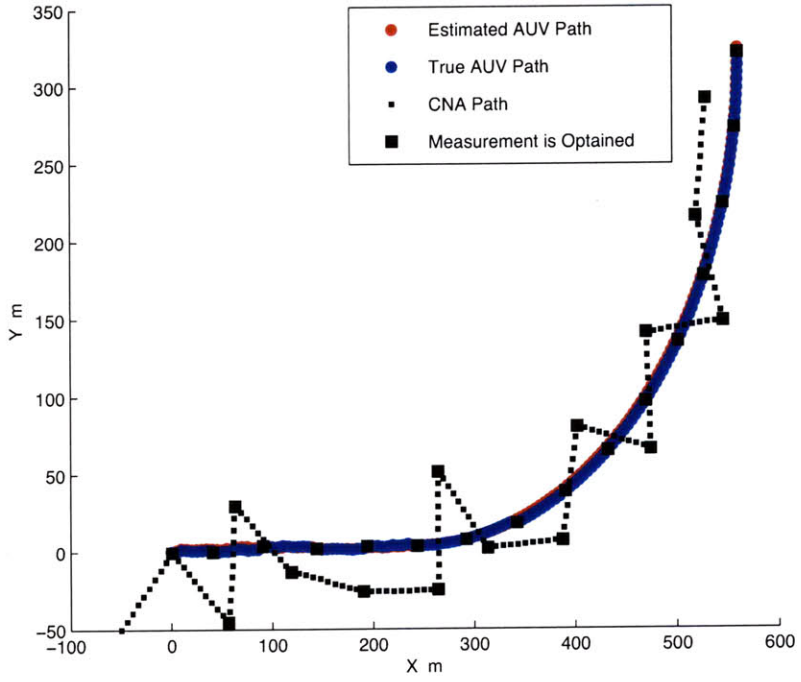

Figure 2-4: Optimal CNA's zig-zag path, is obtained using the approach from [43].

THIS PAGE INTENTIONALLY LEFT BLANK

Chapter 3

Recursive Approaches: Localization With Extended Kalman Filter and Particle Filter

In this chapter, recursive approaches to the localization problem will be discussed. At first we will describe the localization problem as a Bayesian estimation problem. We will also show that under linearity assumptions the problem can be solved recursively in an optimal way; this is the case of Kalman filter. When these assumptions do not hold, then a non-linear method is required. Two of the most commonly used methods are the extended Kalman filter (EKF) and particle filtering. In the EKF, linearization is carried out, leading to the lose of mportant information that can lead to divergence. On the other hand, the performance of particle filtering, which is clearly a non-linear approach, depends on the number of particles used; generally, with a sufficiently high number of particles, it gives better results than the EKF, but is computationally more expensive. More details on the EKF and particle filtering can be found in [35], [32] and [3].

3.1 Probabilistic Framework

The localization problem is typically considered as a Bayesian estimation problem. The real vehicle states are the actual position coordinates, although in our case we need to work in the belief space. The belief space is taken to be the joint probability density function of the vehicle position $X_1 = [x_1, y_1]^T$ over all locations in the vehicle environment Ξ. The belief space is given by Equation (3.1):

$$Bel(X_{1,k}) = P(X_{1,k}|m_0, m_1...m_k) \tag{3.1}$$

where $m_0, m_1...m_k$ are all the measurements gathered by the vehicle up to that time.

All the measurements taken by the robot have to be incorporated under probability laws in order to give correct vehicle position estimates. To make the analysis easier we break the "belief" at each time k into two different beliefs relative to the prior belief ($Bel^-(X_{1,k})$) and to the posterior belief ($Bel^+(X_{1,k})$)

$$Bel^-(X_{1,k}) = P(X_{1,k}|z_1, z_2...z_{k-1}, u_1, u_2...u_{k-1}) \tag{3.2}$$

$$Bel^+(X_{1,k}) = P(X_{1,k}|z_1, z_2...z_k, u_1, u_2...u_k) \tag{3.3}$$

According to [35], using the total probability theorem we can rewrite Equation (3.2):

$$\begin{aligned} Bel^-(X_{1,k}) = \int_{\Xi} & P(X_{1,k}|X_{1,k-1}, z_1, z_2...z_{k-1}, u_1, u_2...u_{k-1}) * \\ & P(X_{1,k-1}|z_1, z_2...z_{k-1}, u_1, u_2...u_{k-1})\, d(X_{1,k-1}) \end{aligned} \tag{3.4}$$

Looking carefully at Equation (3.4) we can say that the second term is the posterior belief of the previous iteration. Using this, Equation (3.4) results in

$$\begin{aligned} Bel^-(X_{1,k}) = \int_{\Xi} & P(X_{1,k}|X_{1,k-1}, z_1...z_{k-1}, u_1, u_2...u_{k-1}) * \\ & Bel^+(X_{1,k-1})\, d(X_{1,k-1}) \end{aligned} \tag{3.5}$$

According to the Markov assumption, the current knowledge of a state depends only on the previous state and the current observations. Using the Markov assumption, the prior belief is simplified to:

$$Bel^{-}(X_{1,k}) = \int_{\Xi} P(X_{1,k}|X_{1,k-1}, u_{k-1}) Bel^{+}(X_{1,k-1})\, d(X_{1,k-1}) \tag{3.6}$$

The above Equation (3.6) gives the prior belief of the robot being in the position $X_{1,k}$, taking into account its previous position $X_{1,k-1}$ and the current velocity measurement. This can be developed to be the prediction step in the Kalman Filter. Up to this point it seems that we have not taken into account any range measurements directly; however, all range measurements up to the previous step have already been taken into account in the computation of the posterior belief in the previous step $Bel^{+}(X_{1,k-1})$.

To incorporate a new range measurement we need to use Bayes' rule. According to Bayes' rule, the posterior belief is equal to the probability of observing the range measurement z_k given that the vehicle is in the state $X_{1,k}$ and all the other measurements taken up to now times the prior of the state are equal to $X_{1,k}$, deviated by the probability of observing z_k given all the information gathered up to now. According to Bayes' rule we have:

$$Bel^{+}(X_{1,k}) = \frac{P(z_k|X_{1,k}, z_1...z_{k-1}, u_1...u_{k-1}) P(X_{1,k}|z_1...z_{k-1}, u_1...u_{k-1})}{P(z_k|z_1..z_{k-1}, u_1...u_{k-1})} \tag{3.7}$$

Using Equation (3.2) we can rewrite Equation (3.7) as

$$Bel^{+}(X_{1,k}) = \frac{P(z_k|X_{1,k}, z_1...z_{k-1}, u_1...u_{k-1}) Bel^{-}(X_{1,k})}{P(z_k|z_1..z_{k-1}, u_1...u_{k-1})} \tag{3.8}$$

Using Markov's assumption we get:

$$Bel^{+}(X_{1,k}) = \frac{P(z_k|X_{1,k}) Bel^{-}(X_{1,k})}{P(z_k|z_1..z_{k-1}, u_1...u_{k-1})} \tag{3.9}$$

Given that all the beliefs are actually probability density functions, it is obviously

correct that:

$$\int_{\Xi} Bel^{+}(X_{1,k})d(X_{1,k}) = 1 \tag{3.10}$$

Using this and some algebra we finally end up with:

$$Bel^{+}(X_{1,k}) = \frac{P(z_k|X_{1,k})Bel^{-}(X_{1,k})}{\int_{\Xi}(P(z_k|X_{1,k})Bel^{-}(X_{1,k}))d(X_{1,k})} \tag{3.11}$$

Equation (3.11) can be used to derive the update steps of the Kalman Filter. Until now we have made no assumptions (Linearity, Gaussian or zero mean noise). If we have an evaluation model that gives $P(z_k|X_{1,k-1}, u_{k-1})$ and a sensor (or perceptual model) model $P(z_k|X_{1,k})$, we can solve the problem. The problem can be as easy or as difficult as solving the integrations in Equations (3.6) and (3.11).

One way to solve these integrals is to discretize the space. This can be done by methods like particle filtering and grid methods, and is something like solving these integrals using arithmetic methods. These methods have no problem dealing with non-linear non-Gaussian pdfs, but are computationally expensive.

Analytical solutions can be given under certain assumptions. In the case of linear Gaussian distributions, a recursive closed form solution exists. This solution is given by the Kalman filter, which minimizes the least-squared error.

3.2 Extended Kalman Filter Localization

3.2.1 Kalman Filter

As we have shown earlier, the state belief can be split into the prior belief Bel^{-} and the posterior belief Bel^{+}. Equations (3.6) and (3.11) give the prior belief and the posterior belief in a way that they can be computed recursively. These two equations under certain assumptions can be developed to be the prediction and the update steps of the Kalman filter.

As stated previously, in the case that both the prior and the posterior remain

Gaussian probability density functions, then the solution of the problem can be given recursively by the Kalman filter equations. For that to hold, there are certain assumptions that the system needs to have regarding system dynamics and the sensor's measurement noise model. We consider the linear Markov process system given by Equations (3.12) and (3.13).

$$X_{1,m} = AX_{1,m-1} + b\omega_{m-1} + N_{m-1} \tag{3.12}$$

$$h_m = HX_{1,m} + n_r \tag{3.13}$$

where $h_m \epsilon R^n$ and where n is the number of observations taken (range measurements in the non-linear case). Control inputs in our case are the velocity measurements and the vehicle heading modeled as random Gaussian variables with mean $\hat{\omega}$ and covariance Ω. In addition, N_m, n_r and the noise involved in the control inputs are random variables introducing noise in the system with the following characteristics: (1) Gaussian; (2) zero mean; and (3) uncorrelated to each other and to themselves.

The prediction step is given by Equation (3.6). Since we assume that the previous posterior remains Gaussian at all times, we can say that to be able to solve the localization problem we need to be able to track the mean and the error covariance of the Gaussian density function. Similarly, in order to derive the update step, we should be able to solve the integrations involved in Equation (3.11), or we should be able to track the mean and the covariance of the posterior belief given that the distributions will always be Gaussians. One easy way to do this is to use Bayes' rule. The actual work done in the update step is to incorporate everything we know until now and incorporate it with the current measurement. A necessary condition of doing this is to have a model to describe the stochastic characteristics of the measurements.

Under linearity and the above assumptions, the Kalman filter is proven to be the observer that minimizes the least square error of all the measurements gathered up the current time. In the Kalman filter derivation we have just described, the optimality of the Kalman filter is not shown. The optimality of the Kalman filter comes from the fact that the prior and the posterior remain Gaussian, and in that

case the Kalman filter is the same as the maximum likelihood estimator, which is essentially the probabilistic point of view of the least-squares estimator.

In the initial derivation of the Kalman filter, Kalman derives the Kalman filter gains by trying to minimize the trace of the posterior covariance matrix. In this problem the objective function is a positively defined quantity in a contractive form, and it is proven that there is only one minimum. Here we do not present the initial derivation because we want to analyze the probabilistic aspect of the problem.

Table 3.1 summarizes the well-known Kalman filter equations [7]. The prediction step is given by the first two lines where the posterior state estimate and the error covariance are computed by propagating the previous posterior estimates of the state and the covariance and incorporating the control inputs u based on the noise free system dynamics. In the prediction step, the determinant of the covariance matrix increases because we add a positively defined matrix $(b\hat{\omega}_{m-1}b^T + Q_{m-1})$ to the initial covariance.

The update step is shown in the last three lines of Table 3.1. In the update step, the state is corrected according to the set of measurements just received. The correction of the state depends on the Kalman gain K and the difference between the measurement h_m and the predicted measurement $\hat{h}_m$. This difference is called the innovation $(\bar{h}_m)$ and is given by:

$$\bar{h}_m = h_m - \hat{h}_m \tag{3.14}$$

In the equation above the measurement is given by Equation (3.13), and the predicted measurement is given by the expected value of the measurement given by the equation:

$$\hat{h}_m = H\hat{X}_{1,m} + E[n_r] \tag{3.15}$$

It is important to note that if the innovation is nearly equal to zero, the update step will have only a small effect on the state estimate; however, it will shrink the error covariance. If the innovation is nearly zero, it means that what the system expects to see is close to what it observes, and therefore there is no reason to change

h

Table 3.1: Kalman filter equations.

$\hat{X}^-_{1,m} = A\hat{X}^+_{1,m-1}$	Prediction
$P^-_m = AP^+_{m,-1}A^T + b\hat{\omega}_{m-1}b^T + Q_{m-1}$	Prediction
$K_m = P^-{}_m H^T (HP^-{}_m H^T + R_m)^{-1}$	Gain
$\hat{X}^+_{1,m} = \hat{X}^-_{1,m} + K_m(h_m - H\hat{X}^-_{1,m})$	Update
$P^+_m = (I - K_m H)P^-_m$	Update

the state estimates. However, the covariance will shrink because now the system is more certain about its estimate, since the expected and predicted observations are the same.

Of course, the innovation will not always be nearly equal to zero. In general, the Kalman filter chooses the gain K to achieve the right balance in weighting the prediction and the innovation. Effectively, the Kalman filter makes a decision on tuning the gain matrix K by looking at and comparing the prior estimated uncertainty and the uncertainty in the observations.

In the case that the measurement noise is small, then the filter makes a decision based mostly on the observation. On the other hand, if the measurement noise is large, then the filter will trust the prediction step more. This can be seen by taking the limits of the Kalman gain when the measurement uncertainty is zero and when the prior covariance is zero.

$$\lim_{P^-_m \to 0} K_m = 0 \tag{3.16}$$

$$\lim_{R_m \to 0} K_m = H^{-1} \tag{3.17}$$

3.2.2 Extended Kalman Filter

We have seen that in the case of linear Gaussian systems the optimal solution is given by the Kalman filter. The Gaussian assumption is reasonable due to the central limit theorem, although the linear assumption is not valid in the general case. In the case that the system is not linear , then linearization can be performed to com-

pute Jacobian matrices, and the estimation problem can be solved using the EKF algorithm [7].

In our case, the system's equation are clearly non-linear and are given by:

$$X_{1,m} = f(X_{1,m-1}, \omega_{m-1}) \tag{3.18}$$

$$h_m = M(X_{1,m}, n_r) \tag{3.19}$$

or

$$\begin{aligned} x_{1,[m+1]} &= x_{1,[m]} + \triangle_m(\hat{v}_m \cos\hat{\theta}_m - \hat{w}_m \sin\hat{\theta}_m) \\ y_{1,[m+1]} &= y_{1,[m]} + \triangle_m(\hat{v}_m \sin\hat{\theta}_m + \hat{w}_m \cos\hat{\theta}_m) \\ h_{[m]} &= \sqrt{(x_{1,[m]} - x_{2,[m]})^2 + (y_{1,[m]} - y_{2,[m]})^2} + n_r \end{aligned} \tag{3.20}$$

In the equations above, the control inputs are the velocity measurements in the forward and the starboard directions plus the vehicle heading taken from the compass. It is imperative to say that in the system above, the process noise N is considered to be zero ($N = 0$), although the control inputs are noisy measurements responsible for the process noise in the system.

$$\omega = [v, w, \theta]^T \tag{3.21}$$

With all these assumptions the Jacobians are given by:

$$F = \begin{pmatrix} 1 & 0 \\ 0 & 1 \end{pmatrix} \tag{3.22}$$

B is the input Jacobian

$$B = \Delta_m \begin{pmatrix} -\sin\hat{\theta} & \cos\hat{\theta} & -(\hat{w}\sin\hat{\theta} + \hat{v}\cos\hat{\theta}) \\ \cos\hat{\theta} & \sin\hat{\theta} & (\hat{w}\cos\hat{\theta} - \hat{v}\sin\hat{\theta}) \end{pmatrix} \tag{3.23}$$

h

Table 3.2: Extended Kalman filter equations

$\hat{X}_{1,m}^{-} = f(X_{1,m-1}, \hat{\omega}_{m-1})$	Prediction
$P_m^{-} = FP_{m-1}^{+}F^T + B\hat{\Omega}_{m-1}B^T + Q_{m-1}$	Prediction
$K_m = P_k^{-}H^T(HP_m^{-}H^T + R_m)^{-1}$	Gain
$\hat{X}_{1,m}^{+} = \hat{X}_{1,m}^{-} + K_k(h_m - h(\hat{X}_{1,m}^{-}))$	Update
$P_m^{+} = (I - K_mH)P_m^{-}$	Update

where H is the output Jacobian defined by:

$$H = \begin{pmatrix} \frac{x_1-x_2}{\sqrt{(x_1-x_2)^2+(y_1-y_2)^2}} & \frac{y_1-y_2}{\sqrt{(x_1-x_2)^2+(y_1-y_2)^2}} \end{pmatrix} \tag{3.24}$$

The above Jacobians are computed using the latest estimated states for each time.

The EKF algorithm is shown in Table 3.2 [7]. In this table, the input covariance is given by:

$$\Omega = \begin{pmatrix} \sigma_{\hat{v}}^2 & 0 & 0 \\ 0 & \sigma_{\hat{w}}^2 & 0 \\ 0 & 0 & \sigma_{\hat{\theta}}^2 \end{pmatrix} \tag{3.25}$$

In addition the range measurement covariance matrix is given by

$$R = {\sigma_r}^2 \tag{3.26}$$

3.3 Particle Filtering

3.3.1 Introduction

The Bayesian estimation localization problem is given by Equations (3.6) and (3.11), which provide the optimal solution. In the case that the integrations in these equations cannot be solved, then we can derive suboptimal solutions. With the assumption of linear models and Gaussian errors, the optimal solution can be given by Kalman filter equations.

In the general case in which the linear Gaussian assumptions do not hold, there are many suboptimal solutions that approximate the solution to the equations (3.11) and (3.11), and therefore approximate the optimal solution to the localization problem. Examples include the EKF (discussed above) and the unscented Kalman filter (UKF) [22].

Particle filtering provides an alternative method for considering the Bayesian estimation problem, without resorting to the assumptions of the EKF or UKF. According to [3], the particle filter is a sequential Monte Carlo method based on point-mass representation of probability densities that can be applied to any state space problem. The first reference to a particle filter goes back to 1940 [42]; however, the first application of the method was performed in the 1980s due to the computational power they demand.

Assuming that the state space is discrete and consists of a finite number of states, then the integrations become summations and the optimal solution for the equations can be given by grid-based methods. According to grid-based methods, the posterior probability is computed for all the states using one particle per state that tracks the posterior probability of the state to be the position which takes into account the process stochastic characteristics and the measurement stochastic characteristics.

Generally, in a real application, the state space is continuous and non-linear, and therefore, the optimal solution to the Bayesian estimation cannot be computed. In addition, the fact that we have to compute the probability of the vehicle being in each state makes grid-based methods computationally too expensive. Another way to get around this problem is to use a set of (N_s) random samples associated with weights; then the estimates can be obtained using these samples and these weights.

Consequently, the particles are considered to be samples of the true posterior distribution, and every single particle i is a hypothesis of where the true state is. At each time the posterior distribution is represented by a set of N_s particles and

weights:

$$\mathbf{X}_{1,k} = [X_{1,k}^{[1]} X_{1,k}^{[2]} ... X_{1,k}^{[N_s]}] \tag{3.27}$$

$$\mathbf{w}_k = [w_k^{[1]} w_k^{[2]} ... w_k^{[N_s]}] \tag{3.28}$$

If all the weights sum up to one then we can say the posterior joint density for all the history of the states up to time k is approximated by Equation (3.29):

$$P(X_{1,0:k}|z_{1:k}, u_{1:k-1}) \approx \sum_{i=1}^{N_s} w_k^i \delta(X_{1,0:k} - X_{1,0:k}^{[i]}) \tag{3.29}$$

where δ in the above expression is the Dirac delta function. The above expression gives the joint probability of all the history of the states; however, we are interested in the posterior probability density function of the current state given all the information gathered up to then. Using Bayes' rule

$$P(X_{1,0:k}|z_{1:k}, u_{1:k-1}) = \frac{P(z_k|X_{1,0:k}, z_{1:k-1}, u_{1:k-1}) P(X_{1,0:k}|z_{1:k-1}, u_{1:k-1})}{P(z_k|z_{1:k-1}, u_{1:k-1})} \tag{3.30}$$

Using Markov assumptions

$$P(X_{1,0:k}|z_{1:k}, u_{1:k-1}) = \frac{P(z_k|X_{1,k}) P(X_{1,0:k}|z_{1:k-1}, u_{1:k-1})}{P(z_k|z_{1:k-1}, u_{1:k-1})}$$

$$= \frac{P(z_k|X_{1,k}) P(X_{1,k}|X_{1,0:k-1}, z_{1:k-1}, u_{1:k-1}) P(X_{1,0:k-1}|z_{1:k-1}, u_{1:k-1})}{P(z_k|z_{1:k-1}, u_{1:k-1})} \tag{3.31}$$

Using again Markov assumptions and simple intuition, we have

$$P(X_{1,k}|X_{1,0:k-1}, z_{1:k-1}, u_{1:k-1}) = P(X_{1,k}|X_{1,k-1}, u_{1:k-1}) \tag{3.32}$$

$$P(X_{1,0:k-1}|z_{1:k-1}, u_{1:k-1}) = P(X_{1,0:k-1}|z_{1:k-1}, u_{1:k-2}) \tag{3.33}$$

Using Equations (3.31), (3.32) and (3.33) we finally have

$$P(X_{1,0:k}|z_{1:k}, u_{1:k-1}) = \frac{P(z_k|X_{1,k})P(X_{1,k}|X_{1,k-1}, u_{1:k-1})P(X_{1,0:k-1}|z_{1:k-1}, u_{1:k-2})}{P(z_k|z_{1:k-1}, u_{1:k-1})} \tag{3.34}$$

It is more convenient to use only the numerator of Equation (3.34)

$$P(X_{1,0:k}|z_{1:k}, u_{1:k-1}) \propto P(z_k|X_{1,k})P(X_{1,k}|X_{1,k-1}, u_{1:k-1}) P(X_{1,0:k-1}|z_{1:k-1}, u_{1:k-2}) \tag{3.35}$$

Equation (3.34) gives the joint probability density function of all the history of the states up to now. It is given as a function of the most recent range and velocity measurements and the history. The measurements (ranges) are taken into account through the weights.

The weights can be computed using the importance sampling principle. According to the importance sampling principle: we assume that $P(X)$ is a pdf that the real samples are supposed to be generated from. This pdf is difficult to compute, and therefore it is difficult to generate samples from it. Due to this fact, we assume that the real samples are generated by another pdf $\pi(X)$ which is analogous to $P(X)$ and is easy to generate samples from. Following Arulampalam *et al.* [3], we assume that samples of the real samples are generated by the importance density $q(.)$. Then the weights are given by:

$$w^i \propto \frac{\pi(X^i)}{q(X^i)} \tag{3.36}$$

Applying Equation (3.36) in our case, we have:

$$w_k^i \propto \frac{P(X_{1,0:k}^i|z_{1:k}, u_{k-1})}{q(X_{1,0:k}^i|z_{1:k}, u_{1:k-1})} \tag{3.37}$$

h

Table 3.3: Summary of particle filtering

$[X^i_{1,k}, w^i_k] = PF([X^i_{1,k-1}, w^i_{k-1}])$
for $i = 1 : N_s$
Draw X^i_k from $q(X_{1,k}\|X^i_{1,k-1}, z_k, u_{k-1}) = P(X_{1,k}\|X^i_{k-1}, u_{k-1})$
$w^i_k = w^i_{k-1} P(z_k\|X^i_{k-1}, u_{k-1})$

It is convenient to factor the importance density as shown in Equation (3.38)

$$q(X_{1,0:k}|z_{1:k}, u_{1:k-1})) = q(X_k|X_{0:k}, z_{1:k}, u_{1:k-1}))(q(X_{1,0:k-1}|z_{1:k-1}, u_{1:k-2})) \quad (3.38)$$

The importance density should be chosen in a clever way. One way to choose it is to try to minimize the variance of the weights [3]. One simple case is to use

$$q(X_{1,k}|X^i_{k-1}, z_k, u_{k-1}) = P(X_{1,k}|X^i_{1,k-1}, u_{k-1}) \quad (3.39)$$

Using the above Equations we end up with:

$$P(X_{1,k}|z_{1:k}, u_{1:k-1}) \approx \sum_{i=1}^{N_s} w^i_k \delta(X_{1,k} - X^{[i]}_{1,k}) \quad (3.40)$$

$$w^i_k \propto w^i_{k-1} P(z_k|X^i_k) \quad (3.41)$$

In Equations (3.40) and (3.41), we cannot see the dependence of the system on the velocity noise directly. However, the velocity measurement noise comes to play through the generation of particles, since the particles are sampled at each time from the $P(X_{1,k}|X_{1,k-1}, u_{k-1})$. The above equations can represent the particle filtering algorithm. We give the results in the Table 3.3.

It is proven that the algorithm above results in almost all particles with nearly zero weights (zero after rounding off), and one particle with a weight close to one. This is called the degeneracy problem. One way to measure the presence of that problem is to examine the number given by Equation (3.42). Small N_{eff} numbers mean the degeneracy problem exists.

$$N_{eff} = \frac{1}{\sum_{i=1}^{N_s}(w_k^i)^2} \tag{3.42}$$

There are two ways to solve the problem; one way is to choose in a clever way the importance density, and the other one is to perform resampling when this number drops below a pre-defined threshold. The method we have adopted for the importance density provides good performance and is convenient to implement. There are a few ways to do resampling; one of the most frequently used ways is to erase the particles whose weights fall below a threshold and to increase the number of particles whose weights are above the threshold. To make the algorithm more robust, we can replace some of the low weight particles with some random particles.

3.3.2 Application of PF to the Localization Problem

The algorithm is constituted by 4 steps; these steps are the initialization, the prediction, the update and resampling. In the initialization step we compute the initial cloud of particles and the initial weights. The initial cloud of particles is drawn by a Gaussian pdf with a mean of the GPS reading and a variance the GPS variance. All weights are considered to be the same and normalized to sum up to one.

In the prediction step, all the particles are propagated according to the process model. Each particle is computed using control inputs (velocities) drawn from a normal distribution with a mean of the associated measurement and standard deviation equal to 0.5 m/s.

$$x_{1,m}^{[i]} = \hat{x}_{1,m-1} + (v_{m-1}\cos\theta - w_{m-1}\sin\theta)\Delta_m \tag{3.43}$$

$$y_{1,m}^{[i]} = \hat{y}_{1,m-1} + (w_{m-1}\cos\theta + v_{m-1}\sin\theta)\Delta_m \tag{3.44}$$

Then the predicted position of the vehicle can be given by the weighted mean of all the particles. The way that the estimated position is generated using the particles and the weights is really important. There are a few ways in which this can be done,

and each of them gives good results for different problems. The three more commonly used ways are:

- the weighted mean is chosen (this is good for unimodal distributions);
- the best particle (the one with the largest likelihood) is chosen; or,
- the mean of the best group of particles is chosen.

In our case the distributions are typically not multimodal; therefore good performance has been achieved using the weighted mean given by Equations (3.45) and(3.46)

$$\hat{x}_{1,m}^{-} = \frac{\sum_{i=1}^{N_s} w_{m-1}^{i} x_{1,m}^{[i]-}}{N_s} \tag{3.45}$$

$$\hat{y}_{1,m}^{-} = \frac{\sum_{i=1}^{N_s} w_{m-1}^{i} y_{1,m}^{[i]-}}{N_s} \tag{3.46}$$

The update step takes into account the range measurements. Using the stochastic characteristics of the sensor we update the weights. The idea is simple — the survival of the fittest. Particles that are close to the range measurement receive larger weights and particles that are farther from the range measurement are assigned smaller weights. This can be done using the likelihood density defined by Equation (3.47)

$$L^{[i]} = P(z_m - \hat{h}_m^{[i]} | X_{1,m-1}^{i}, u_{m-1}) \tag{3.47}$$

where h_m is the range measurement and $\hat{h}_m^{[i]}$ is the predicted range measurement for each particle defined as:

$$\hat{h}_m^{[i]} = \sqrt{(X_{1,m}^{[i]-} - X_{2,m})^T (X_{1,m}^{[i]-} - X_{2,m})} \tag{3.48}$$

The likelihood is taken to be a Gaussian pdf with mean equal to the innovation and variance equal to the variance of the range measurements; therefore, the likelihood of

each weight is computed through Equation (3.49)

$$L^{[i]} = \frac{1}{\sqrt{2\pi R}} e^{\frac{-(h_m - \hat{h}_m^{[i]})^2}{2R}} \tag{3.49}$$

Having the new likelihood for each particle, we can compute the new weights and the new estimated positions using the weighted mean described in Equations (3.45) and (3.46). The new weights are given by:

$$w_m^i = w_{m-1}^i L^{[i]} \tag{3.50}$$

As we said earlier, if we keep doing predictions and continuously updating, then some particles will drift far apart and will end up with zero weights. If a particle obtains a zero weight (after round off), then it can never obtain a nonzero weight even if the range measurements are close to these particles. In order to prevent that from happening, we conduct resampling. Resampling is the operation by which we delete all the particles and their weights and draw new particles. The new particles have all the same weights equal to $1/N_s$, and they are drawn in the way described in the paragraph above. Resampling should be done only when the effective sample size, defined by the Equation (3.42) reaches a threshold. This threshold is a function of the number of particles used. For a large number of particles this threshold is set to be low. On the other hand, the fact that we do not have a lot of range measurements forces us to keep this threshold as a large number.

3.4 Summary

This chapter has reviewed the two basic recursive state estimators — the EKF and particle filtering — that we have considered for the cooperative localization problem. Before describing the performance of these approaches with real experiments, in the next chapter we will first describe an alternative approach based on nonlinear optimization.

Chapter 4

Non-Linear Least Squares

An alternative to the recursive state estimators discussed in the previous chapter is to perform an incremental batch optimization which computes the trajectory that minimizes the least square error of the complete proposed state trajectory relative to the measurements. In the Gaussian (linear or non-linear) case, this is equivalent to the Maximum Likelihood Estimator (MLE).

4.1 Least Squares Formulation

To consider the MLE estimator, all the vehicle position measurements should be included in the optimization. Given that velocity measurements are taken approximately 50 times more frequently than the range measurements; it is common to group all the velocity measurements between two sequential range measurements $(h_{[i-1]}, h_{[i]})$ into one cumulative dead-reckoning measurement $(z_{o,[i]} = [\Delta X_{[i]}, \Delta Y_{[i]}]^T)$. This allows us to reduce the number of states in the optimization to a reasonable number.

Figure 4-1 shows a series of poses of the AUV and the surface vehicle. At time $t = 0$, both the surface vehicle and the AUV have a certain initial location estimate with a known uncertainty. At some time later, $t = 1$, the AUV has moved to another location and receives a range measurement from the surface vehicle, $h_{[1]}$. Between these times the AUV computes a cumulative dead-reckoning vector using forward and starboard velocity measurements as well as compass heading estimates. This vector

will be denoted $z_{o,[1]}$.

After n such periods, our aim is to compute the trajectory, $X_{1,[1:n]}$, that minimizes the least squares error of all cumulative dead-reckoning measurements, $z_{o,[1:n]}$, the range measurements, $h_{[1:n]}$ and surface vehicle GPS locations, $X_{2,[1:n]}$, up to the current time.

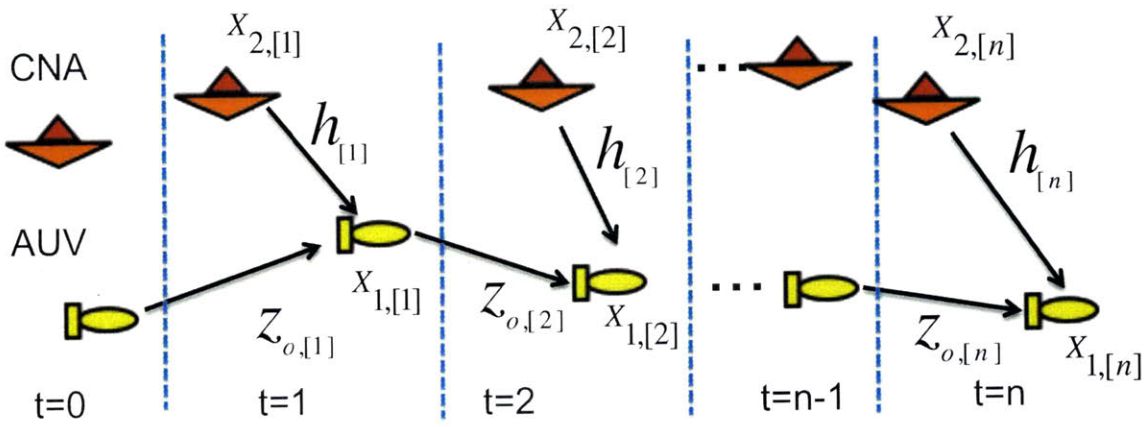

Figure 4-1: Least Squares framework for a series of poses.

The trajectory corresponding to the least squares error can be found by minimizing

$$(X_{1,[1:n]})^* = \underset{X_{1,[1:n]}}{\operatorname{argmin}}(C_{(X_{1,[1:n]})}) \tag{4.1}$$

with the following cost function

$$C = \frac{1}{2}\sum_{i=1}^{n}(||(X_{1,[i]} - X_{2,[i]})|| - h_{[i]})^T \Sigma_{r,[i]}^{-1}(||(X_{1,[i]} - X_2[i])|| - h_{[i]}) + \frac{1}{2}\sum_{i=1}^{n}(X_{1,[i]} - X_{1,[i-1]} - z_{o,[i]})^T \Sigma_{o,[i]}^{-1}(X_{1,[i]} - X_{1,[i-1]} - z_{o,[i]})$$

where the covariance of the odometry measurements are

$$\Sigma_{o,[i]} = \begin{pmatrix} \sigma_{o,xx,[i]}^2 & 0 \\ 0 & \sigma_{o,yy,[i]}^2 \end{pmatrix} \tag{4.2}$$

and the range range measurement is

$$\Sigma_{r,[i]} = \sigma_r^2 \tag{4.3}$$

Before describing our implementation of the NLS estimator for cooperative localization, in the next section we first discuss the issue of convergence.

4.2 Convexity Analysis

One important property for this optimization is convexity — that is if an objective function is convex then it has a single global minimum (or maximum) that can be found by using any optimization method that follows the gradient of the function. One way to determine convexity is through a study of the Hessian matrix of the cost function. If the Hessian matrix is a positive definite matrix, then the objective function is a convex function.

Convexity of a non-linear least squares problem is a very difficult problem to be solved and in the general case convexity is almost impossible to be proven; however by making some reasonable assumptions the convex area of the non-linear least square problem that includes the global minima can be identified.

We now describe and justify the assumptions we have made in our approach for analyzing the convexity of NLS for this problem. First, we make a major assumption – in contrast to the previous chapters, in which standard Gaussian errors are assumed, we will now assume that we have *bounded* non-Gaussian zero mean random noise on the range and the cumulative dead-reckoning measurements. In this case, the following equations will hold.

$$h_{real} - \epsilon_r < h_{r,1} < h_{real} + \epsilon_r \tag{4.4}$$

$$||X_{1,real}|| - \epsilon_o < ||X_1|| < ||X_{1,real}|| + \epsilon_o \tag{4.5}$$

These conditions are essential for the remainder of the analysis in this chapter.

Next, we also assume that the cumulative dead-reckoning variance is much bigger

than the range measurements variance. This assumption is reasonable in the case we use inexpensive dead reckoning sensors, as in the current work. We also assume non-Gaussian isotropic zero mean bounded random noise on the cumulative dead-reckoning measurements. The variance in the x direction is the same as the y direction for a short period of dead reckoning as the measurement variances which were used to form them, $\sigma_v^2 = \sigma_w^2$, are derived from the same sensor and are significantly more uncertain that the heading uncertainty σ_θ^2. This leads to a circular uncertainty for each dead-reckoning portion (see Equation 2.5). We also assume that the dead-reckoning noise is also bounded noise by a circle of radius ϵ_o.

4.2.1 Convexity Analysis for an n-Pose System

The Hessian matrix (H) is defined as the square matrix of the second-order partial derivatives of the objective function. First we shall decompose the Hessian into two different matrices: the contribution of the dead-reckoning measurements (H_o) and the contribution of the range measurements (H_r). Thus the Hessian becomes

$$H = H_r + H_o \tag{4.6}$$

where

$$H_o = \begin{pmatrix} \lambda_1+\lambda_2 & 0 & -\lambda_2 & 0 & 0 & 0 & 0 & 0 \\ 0 & \lambda_1+\lambda_2 & 0 & -\lambda_2 & 0 & 0 & 0 & 0 \\ -\lambda_2 & 0 & \lambda_2+\lambda_3 & 0 & -\lambda_3 & 0 & 0 & 0 \\ 0 & -\lambda_2 & 0 & \lambda_2+\lambda_3 & 0 & -\lambda_3 & 0 & 0 \\ \vdots & \vdots & \vdots & \vdots & \vdots & \vdots & \vdots & \vdots \end{pmatrix}$$

and

$$\lambda_i = \frac{1}{\sigma_{o,[i]}^2} \tag{4.7}$$

while

$$H_r = \begin{pmatrix} A_1 & \Gamma_1 & 0 & 0 & ... & 0 & 0 \\ \Gamma_1 & B_1 & 0 & 0 & ... & 0 & 0 \\ 0 & 0 & A_2 & \Gamma_2 & ... & 0 & 0 \\ 0 & 0 & \Gamma_2 & B_2 & ... & 0 & 0 \\ \vdots & \vdots & \vdots & \vdots & \ddots & \vdots & \vdots \\ 0 & 0 & 0 & 0 & 0 & A_n & \Gamma_n \\ 0 & 0 & 0 & 0 & 0 & \Gamma_n & B_n \end{pmatrix}$$

with

$$\begin{aligned} A_i &= \left(1 - h_{[i]} \frac{(y_{1,[i]} - y_{2,[i]})^2}{\bar{h}_{[i]}^{1.5}}\right) \sigma_{r,[i]}^{-2} \\ B_i &= \left(1 - h_{[i]} \frac{(x_{1,[i]} - x_{2,[i]})^2}{\bar{h}_{[i]}^{1.5}}\right) \sigma_{r,[i]}^{-2} \\ \Gamma_i &= h_{[i]} \frac{(x_{1,[i]} - x_{2,[i]})(y_{1,[i]} - y_{2,[i]})}{\bar{h}_{[i]}^{1.5}} \sigma_{r,[i]}^{-2} \end{aligned}$$

using

$$\bar{h}_{[i]} = ((x_{1,[i]} - x_{2,[i]})^2 + (y_{1,[i]} - y_{2,[i]})^2)$$

A necessary and sufficient condition for the system to be convex is given by

$$(X_{1,[1:n]})^T (H_r + H_o)(X_{1,[1:n]}) > 0 \tag{4.8}$$

The function can be decomposed into two terms: the first term is due to the dead reckoning contribution

$$\begin{aligned} K &= (X_{1,[1:n]})^T (H_r)(X_{1,[1:n]}) \\ &= \lambda_{o,1}(x_1^2 + y_1^2) + \\ &\quad \sum_{i=1}^{n-1} \lambda_{o,i+1}(x_i^2 + x_{i+1}^2 - 2x_i x_{i+1} + \\ &\quad y_i^2 + y_{i+1}^2 - 2y_i y_{i+1}) \end{aligned} \tag{4.9}$$

and the second which is due to the range measurement

$$\begin{aligned} M &= (X_{1,[1:n]})^T (H_o)(X_{1,[1:n]}) \\ &= \sum_{i=1}^{n} (A_i x_i^2 + B_i y_i^2 + 2\Gamma_i x_i y_i) \end{aligned} \tag{4.10}$$

Using the inequality $x_i^2 + x_{i+1}^2 > 2x_i x_{i+1}$, it can be seen that K (the dead-reckoning contribution to the objective function) is always positive. However, the entire Hessian is not positive definite since M (the range contribution) is not positive.

4.2.2 Convexity for a Single Pose

If a system of n poses is not convex that means that we cannot be certain that any optimization method will converge to the global minimum. Instead we aim to solve the problem by calculating a region of attraction (a convex area in the objective function) that includes the global minimum. To do this for a system of n poses is a multi-dimensional search problem. Instead of solving for all n poses at once, we propose to solve the problem sequentially. By doing so, we can simplify the problem in such as way as to include only one pose optimization per iteration and then we will generalize the results for the whole problem.

First we consider the case in which we have only one set of range measurements and one dead-reckoning vector. The Hessian of this subsystem of one pose is given by:

$$H_{[1]} = \begin{pmatrix} A_1 + \lambda_1 & \Gamma_1 \\ \Gamma_1 & B_1 + \lambda_1 \end{pmatrix} \tag{4.11}$$

For the Hessian to be positive definite, $\det(H_{[1]})$ needs to be positive

$$\det(H_{[1]}) = (A_1 + \sigma_{o,1}^{-2})(B_1 + \sigma_{o,1}^{-2}) - \Gamma_1^2 \tag{4.12}$$

We will consider the conditions or region for which this holds. Substituting for A_1, B_1 and Γ_1, we conclude that the region for which the Hessian is positive definite if

characterized by the inequality below

$$\sigma_{r,1}^{-2} + \sigma_{o,1}^{-2} > \frac{\sigma_{r,1}^{-2} h_{r,1}}{\sqrt{((x_1 - x_2)^2 + (y_1 - y_2)^2)}} \tag{4.13}$$

Assuming that the range measurements are bounded by circle of radius ϵ_r, $h_{\text{real}} - \epsilon_r < h_{r,1} < h_{\text{real}} + \epsilon_r$, the worst case scenario is:

$$h_{r,1} = h_{real} + \epsilon_r \tag{4.14}$$

Combining these equations we can compute the area for which $\det(H_{[1]})$ is positive, and the Hessian is positive definite. This area is given by

$$\sqrt{(x_1 - x_2)^2 + (y_1 - y_2)^2} > \frac{h_{real} + \epsilon_r}{1 + (\frac{\sigma_r}{\sigma_{o,1}})^2} \tag{4.15}$$

Given a circular bound of radius $\epsilon_{o,1}$ on dead reckoning measurements, the following holds

$$h_{\text{real}} - \epsilon_{o,1} < \sqrt{(x_1 - x_2)^2 + (y_1 - y_2)^2} < h_{\text{real}} + \epsilon_{o,1}$$

Taking again the worst case scenario

$$h_{\text{real}} > \frac{\epsilon_{o,1}(1 + \Lambda) + \epsilon_r}{\Lambda} \tag{4.16}$$

where:

$$\Lambda = (\frac{\sigma_{r,1}}{\sigma_{o,1}})^2 \tag{4.17}$$

We assert that if these two assumptions hold and the dead-reckoning vector is chosen as the initial condition, $\det(H_{[1]})$ is positive and the resultant objective function is convex.

Consider the above equation: if the range measurement variance is small compared to the dead reckoning measurement variance, then the convex area will become smaller as the estimation is based mostly on the range measurements (as the range

measurements cause the non-convex objective function behavior). In the limit, when the variance of the range measurements goes to zero, Equation 4.16 will never hold. On the other hand when the variance of the dead reckoning goes to zero, Equation 4.16 will almost always hold.

Figure 4-2 visualizes a side view of the contribution of dead-reckoning and range to the NLS objective function in Equation 4.2. The range contribution is non-convex, and the dead-reckoning contribution is convex. When dead-reckoning has small variance, as is shown for Figure 4-2 in the left , the total cost is also convex and the system is guaranteed to converge. However when dead-reckoning has large variance, the objective function may include regions where the contribution of range measurements to NLS is non-convex. This can possibly lead to the overall objective function being non-convex and thus the NLS algorithm may fail to converge to the global minimum.

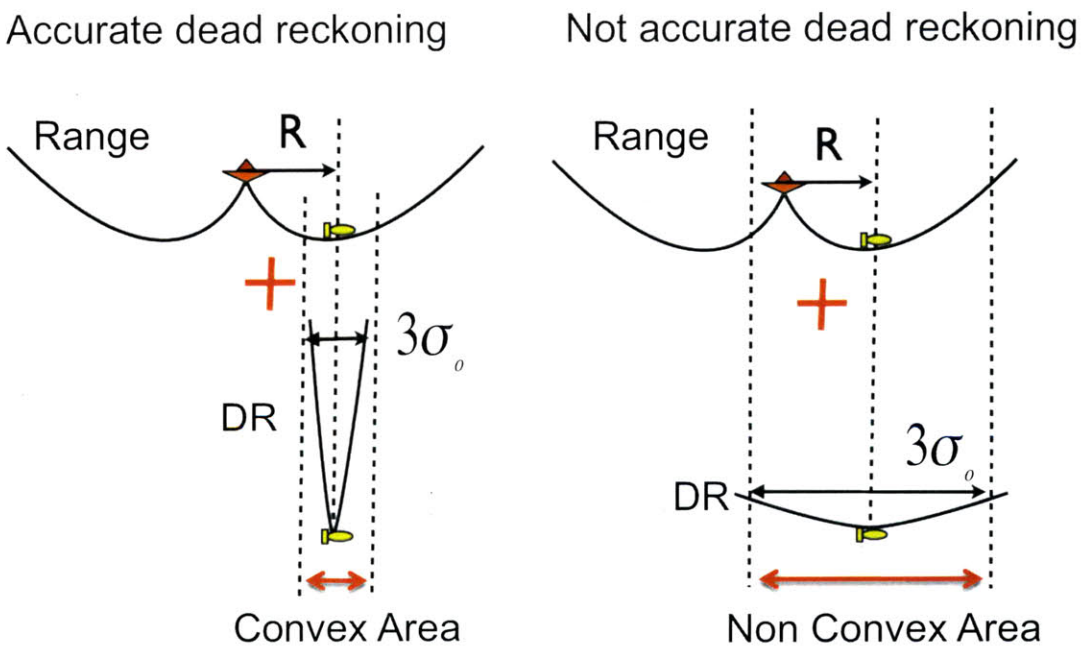

Figure 4-2: The objective function is the combination of range and dead-reckoning contributions. For the case shown on the left, an accurate dead-reckoning system will ensure that NLS optimization converges to the global minimum; for the case shown on the right, inaccurate dead-reckoning can lead to convergence in a local minimum only.

4.2.3 Generalization to the Full System

If we consider only one pose and Equation 4.16 holds, then the dead-reckoning places the system in a convex area. By generalizing this single-pose solution, we hope to solve this same problem for n poses in sequential fashion by arguing that the objective function of the subsystem has the same characteristics as the objective function of the entire system if solved. If this is so the same condition holds for all the subsystems.

Consider the case in which we have sequentially optimized up to $n-1$ poses and a new set of range and dead-reckoning measurements has been received. In this case the objective function is a contribution of n range measurement terms and n dead-reckoning terms

$$\begin{aligned} C &= C_{r,1:n} + C_{o,1:n} \\ &= \sum_{i=1}^{n-1}(C_{r,i} + C_{o,i}) + C_{r,n} + C_{o,n} \end{aligned}$$

Since we have optimized up to the $n-1$ pose, the terms $\sum_{i=1}^{n-1}(C_{r,i} + C_{o,i})$ have minimum value $C_{r,min} + C_{o,min}$. If now we include in the optimization the nth pose, then we may be able to find a different solution that gives smaller $C_{o,min}$ since there is a weak coupling of the dead-reckoning between the poses. Nonetheless, the range measurements will penalize the objective function as there is no coupling between the poses and at the same time the range measurement variance is much smaller than the dead-reckoning variance. By induction, we can show that by solving the problem sequentially, the objective function will have the same characteristics (topology) as that of a simple subsystem.

We have derived Equation 4.16 assuming that the vehicle's initial position is known. If the vehicle's initial position is unknown, then Equation 4.16 is invalid. However, if the vehicle's initial position is unknown but bounded, then Equation 4.16 is valid if the dead-reckoning bound is increased to account for the uncertainty of the previous position. Then the condition for the second subsystem to be convex will

now become

$$h_{\text{real}} > \frac{\epsilon_{o,*}(1+\Lambda)+\epsilon_r}{\Lambda} \tag{4.18}$$

$$\epsilon_{o,*} = \epsilon_{o,1} + (||\epsilon_1 - c_1||)^2 \tag{4.19}$$

where ϵ_1 is the dead-reckoning error vector and c_1 is the correction after the optimization. After a few poses the condition will be

$$h_{\text{real}} > \frac{\epsilon_{o,*}(1+\Lambda)+\epsilon_r}{\Lambda} \tag{4.20}$$

$$\epsilon_{o,*} = \epsilon_{o,1} + (||\epsilon_1 + \epsilon_2 ... \epsilon_n - (c_1 + c_2 + ... + c_n)||)^2$$

Assuming zero mean noise, the errors ϵ_i and the corrections c_i are random variables with zero means with an expected sum of zero

$$\mathbb{E}(||\epsilon_1 + \epsilon_2 ... \epsilon_n - (c_1 + c_2 + ... + c_n)||) = 0 \tag{4.21}$$

and

$$\begin{aligned}\mathbb{E}(\epsilon_{o,*}) &= \mathbb{E}(\epsilon_{o,1}) \\ &\quad + (\mathbb{E}(||\epsilon_1 + \epsilon_2 ... \epsilon_n - (c_1 + c_2 + ... + c_n)||))^2 \\ &= \mathbb{E}(\epsilon_{o,1})\end{aligned}$$

Based on the argument presented above, we propose the following algorithm to solve the problem:

1. Form an optimization problem that minimizes the least squares error for all the measurements taken up to the current time

2. Use as the initial condition to the optimization the previous optimal solution plus the extra pose from the current odometry measurement

3. Minimize the cost function using any gradient method[1]

[1]Conjugate gradient methods are preferred, as their "banana-shape" qualities best fit our pre-

4. If a new range measurement is received, compute the cumulative dead-reckoning vector, increase the number of poses, and repeat.

Assuming bounded noise and that condition in Equation 4.16 holds, then the optimization algorithm will always start within the convex area that includes the global minimum.

In the above analysis we considered bounded noise. It is obvious that in the case that the noise is not bounded, we cannot guarantee convergence. This the case of a system with Gaussian noise (the Gaussian noise is by definition unbounded); however by considering an $n\sigma$ bound on the range and odometry measurements, and by choosing not to use a measurement that lies outside of the bounds (outlier rejection based on the vehicle's predicted location), it may be possible to assure convergence to the global minima. In the Gaussian case, assuming $n\sigma$ bound on the range and odometry measurements, the convergence criterion is given by the following equation:

$$h_{real} > n\left(\frac{\sigma_{o,1}^2}{\sigma_r} + \frac{\sigma_{o,1}^3}{\sigma_r^2} + \sigma_{o,1}\right) \tag{4.22}$$

It is important to notice that, in the Gaussian linear case a unique solution exists and is given by the well known Kalman filter. According to our results, Equation 4.16 (in the general case) and Equation 4.22 (in the Gaussian case), the existence of a unique solution depends on noise characteristics. The only case that the unique solution existence is independent on the noise characteristics (both in the Gaussian and in the general case) is the case that the range measurements tend to infinity. If the range measurements tends to infinity they appear to be straight lines, resulting in a linear system; this agrees with Kalman's results.

4.3 Summary

This chapter has presented an NLS approach to cooperative localization, with a convexity analysis based on the assumption of bounded measurement errors. Next, the

ferred objective function.

following chapter will present our experimental results comparing the different estimators that we have discussed.

Chapter 5

Experiments and Results

The approaches that we have described in the previous chapters have been tested and evaluated in several experiments in the Charles River, using robotic kayaks, acoustic modems, and a small low-cost AUV. In this chapter we describe the hardware used in the experiments and we present results obtained using the EKF, PF and NLS estimators. As expected, the NLS algorithm outperforms the other methods.

5.1 Hardware

5.1.1 Robotic Platforms

Our algorithms were tested on in two different types of experiments, using real acoustic range data. In the first experiment, we used one robotic kayak in the ASV role and a second one simulating the AUV. In the second experiment we used a robotic kayak and an OceanServer Iver2 underwater vehicle. In Figure 5-1, we can see a robotic kayak and the underwater vehicle used in the second experiment; similar experimental results can be found in Fallon *et al.* [13].

All vehicles used in the experiments run MOOS-IvP [8], giving them the capability to make decisions autonomously. The kayaks are equipped with GPS to be able to know their locations. A proportional-derivative path controller runs on each kayak, providing motion along desired trajectories. The controller takes as feedback the

(a)

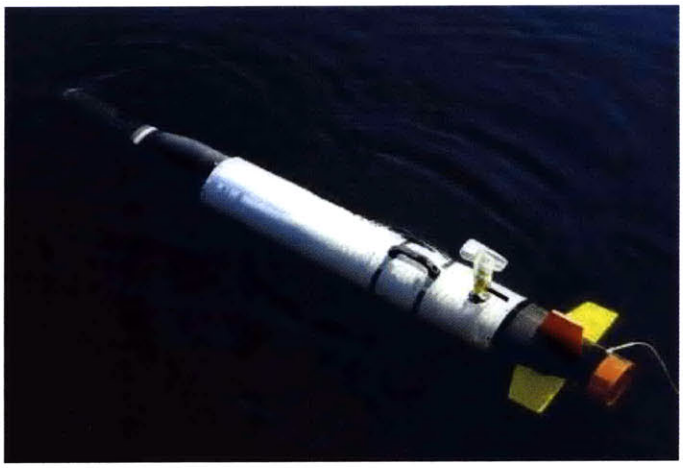

(b)

Figure 5-1: The autonomous vehicles we consider in this thesis: (a) MIT SCOUT autonomous kayaks; (b) the OceanServer Iver2 AUV.

vehicle's position through the GPS to close the control loop. The kayak's forward velocity is in the range of 2-3 m/s for these experiments.

5.1.2 Acoustic Communications and WHOI Micro-modems

Two different methods are used to communicate with the kayaks: wireless ethernet and underwater acoustic modems. Wireless ethernet is used to control and monitor the experiment and the acoustic modems are used by the kayaks for ranging and to transmit data packets to one another. In this way, we duplicate the real scenario of using underwater vehicles, in a more convenient testbed.

In the acoustic communication community, researchers have developed two primary modulation techniques, Frequency Shift Keying (FSK) and Phase Shift Keying (PSK) [24]. Both techniques present advantages and disadvantages. The main advantages of FSK modulation is that it provides robust performance in a noisy environment. However, the main disadvantage of the FSK is that in an ideal case we can only transmit 0.5 sym/Hz; meaning, the efficiency is low. In comparison, the main advantage of the PSK approach is that the efficiency is higher. In an ideal case we can transmit 1 sym/Hz. The main disadvantage of PSK, however, is that in order to decode a message we need to run estimation algorithms to track the acoustic channel. This makes PSK modulation more sensitive to noise and the effects of multipath.

In both cases, the amount of data broadcast is limited by the available acoustic bandwidth. The bandwidth is defined as the range of frequencies we can transmit a signal at for which the power of the signal remains above 3 db. Since the bandwidth depends on the dynamics of the transmission and the environment, there is nothing we can do about it. For our application we use the FSK mode because we operate in a noisy environment, and we wish to maximize the probability of receiving the message. In our case the bandwidth is about 12 kHz and the carrier frequency is 20 Khz. A detailed description of the WHOI micro-modem can be found in [14]. A photo of the main processor board of the micro-modem is shown in Figure 5-2.

The communication cycle proceeds as follows:

- The surface vehicle transmits a ping to the underwater vehicle to inform that it is ready to transmit a data packet.
- The underwater vehicle is ready to receive data.
- Surface vehicle sends a 32 byte packet containing its position, its covariance and several other pieces of information.
- If the underwater vehicle receives the packet, it computes the relative range measurement and then it uses the information gathered to estimate its position.

As stated earlier, we use the micro-modems not only to broadcast information

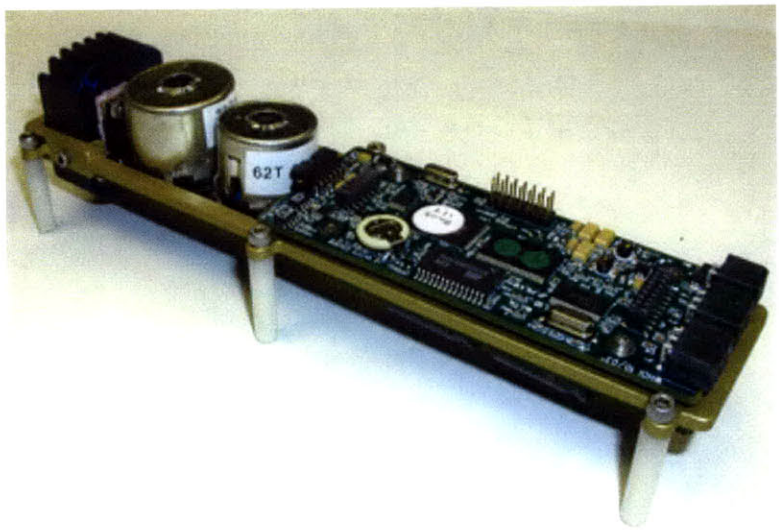

Figure 5-2: The WHOI micro-modem.

but also to measure relative range measurements between the surface vehicle and the underwater vehicle. We assume that all vehicles are time-synchronized with one another. Therefore, we can compute the travel time of the acoustic transmission, and multiply this time by the sound velocity in the water to estimate the range between the two vehicles.

From the experimental data, the errors in the range measurements appear to be well modeled with a zero-mean Gaussian distribution. In the figure below we can see a plot of the error $E = h - h_{real}$. The "real" range measurement for comparison is estimated by GPS. In an estimation problem we need to know the stochastic characteristics of the sensor used in the experiments.

Here we try to characterize the modems with respect to the ranges they give. We use two sets of experiments. In the first experiment, the range measurements can be taken to be Gaussian with a mean equal to -0.07m and standard deviation equal to 5m. In the second experiment, the range measurements can also be taken to be Gaussian with a mean equal to 0.45m and standard deviation equal to 4.27m. We can see their characteristics in Figure 5-3.

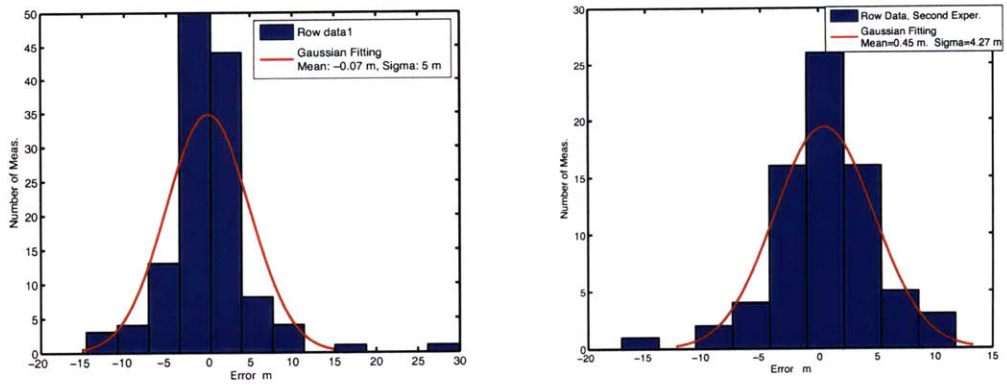

(a) Dataset1 (b) Dataset2

Figure 5-3: Modem characterization: Gaussian fitting.

5.2 Experimental Results

5.2.1 Experiments Description

A set of experiments was carried out in the Charles River near MIT to demonstrate the cooperative ASV/AUV localization problem and to evaluate our algorithm. In Figure 5-4 we can see a top view of the operational area of the robots in the Charles River, indicated by a yellow box. The operating region had an area of several square kilometers. Figure 5-5 shows one of the kayaks in the Charles River operating area. In these experiments, the underwater vehicle moved in a box pattern and the surface vehicle was following behind in a zig-zag pattern.

The range measurements are characterized by a Gaussian with $\sigma_r = 5m$. The vehicle heading uncertainty was taken to be $\sigma_\theta = 3^o$. As the vehicles did not have velocity sensors differential GPS measurements were used to produce simulated velocity measurements. We envisage our solution to be used with a low cost AUV (such as the OceanServer Iver2 shown in Figure 5-1) with imprecise actuation sensors. Modeling this scenario, we choose the forward and starboard velocity measurement variances to be $\sigma_{\hat{v}} = \sigma_{\hat{w}} = 0.5m/s$.

In this experiment, we present both vehicles navigating autonomously and running an online EKF MLBL algorithm. Figure 5-6 shows how the simulated AUV moved in a box pattern, while the surface vehicle followed a zig-zag pattern behind it. (Its

Figure 5-4: The operational area for the experiments, in the Charles River near MIT.

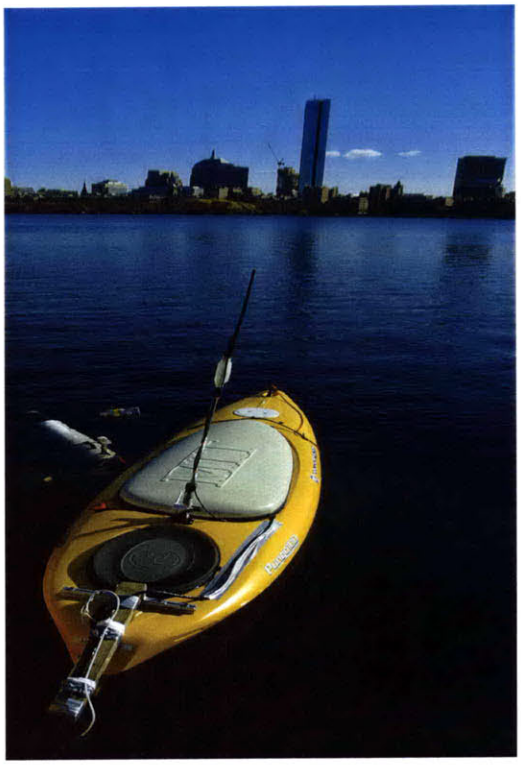

Figure 5-5: An autonomous kayak performing a mission at our test site.

path is not shown here). The supporting vehicle's path was chosen so as to maximize the observability of the system.

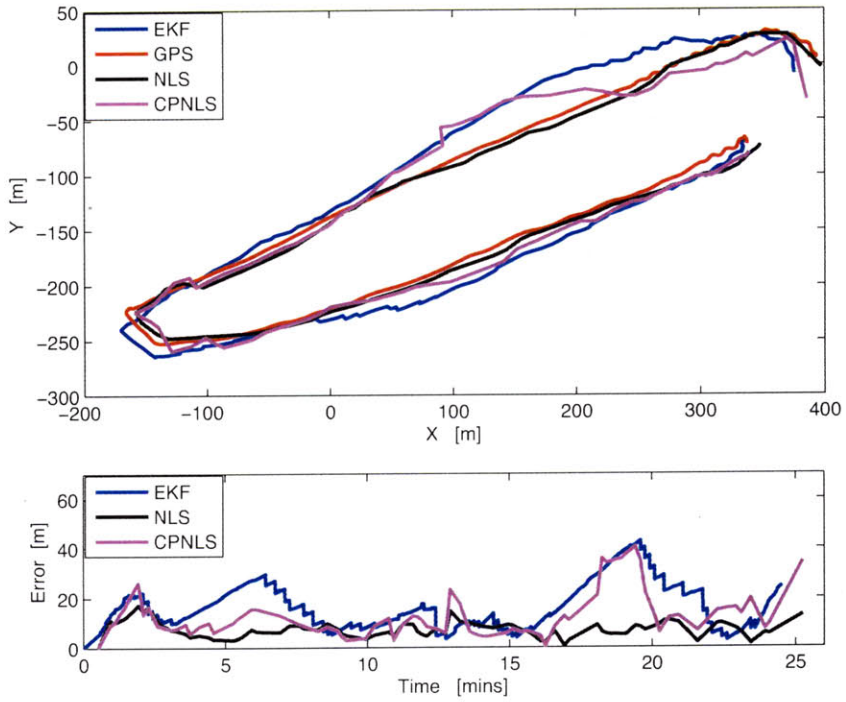

Figure 5-6: Comparison of different localization methods.

5.2.2 Experimental Results Using Two Kayaks

In this subsection, we present experimental results for the cooperative localization problem using two kayaks. We give results with several different state estimators – the EKF, particle filtering, and NLS. The results demonstrate the superior performance of the NLS estimator.

In Figure 5-6 and Table 5.1 we can see a comparison between our proposed NLS algorithm and the commonly used EKF and particle filter. Two mean error values are presented for the NLS. One is the mean error for the entire optimization over the full trajectory (NLS) which would not have been available to the AUV for mission planning as it requires the full set of measurements — including future measurements to be calculated. The second is the mean error of each NLS estimate at the time it

was first calculated. We term this the current point non-linear least squares (CPNLS) estimate.

Our results show that the NLS and CPNLS outperform the EKF, as expected. The CPNLS estimate only marginally outperforms the particle filter, but as discussed earlier, the CPNLS is a more desirable non-stochastic system for this applications. Admittedly, the number of states included in NLS optimization increases continuously, and as a result the required computation increases accordingly. Post processing the data we gathered, we verified that the NLS localization algorithm runs in real-time for missions of length $O(1hr)$. In future work will consider efficient incremental implementations of the NLS such as iSAM [23].

Table 5.1: Comparison of different localization methods.

Method	Mean Error
EKF	18.84m
PF	13.65m
CPNLS	13.12m
NLS (post)	8.94m

In Figure 5-7, we present the localization error for the NLS solution for this experiment (upper figure), the eigenvalues of the observability matrix (center figures) and in the lower figure the convexity criterion in Equation 4.16 expressed as a ratio

$$G(i) = \frac{h_{\text{real},[i]}}{3\left(\frac{\sigma^2_{o,[i]}}{\sigma_{r,[i]}} + \frac{\sigma^3_{o,[i]}}{\sigma^2_{r,[i]}} + \sigma_{o,[i]}\right)} \tag{5.1}$$

If this criterion is smaller than one, then convexity is not guaranteed. We can see that typically, the convexity criterion holds and the error is bounded and related to the sensor variance. On occasion, however, the localization error increases when the eigenvalues of the observability matrix are small, and hence the criterion is below unity. The eigenvalues of the observability matrix provide a way to see if a range measurement is informative enough to recover the vehicle's position. Examining the eigenvalues, we can see that one of the two eigenvalues dominates. The first eigenvalue

is in the range from 50 to 100, and the second eigenvalue is in the range from 0 to 10. This is due to the configuration of the experiment.

Since the first eigenvalue dominates then if the first eigenvalue becomes small then the error increases, this can be seen in the Figure 5-7.

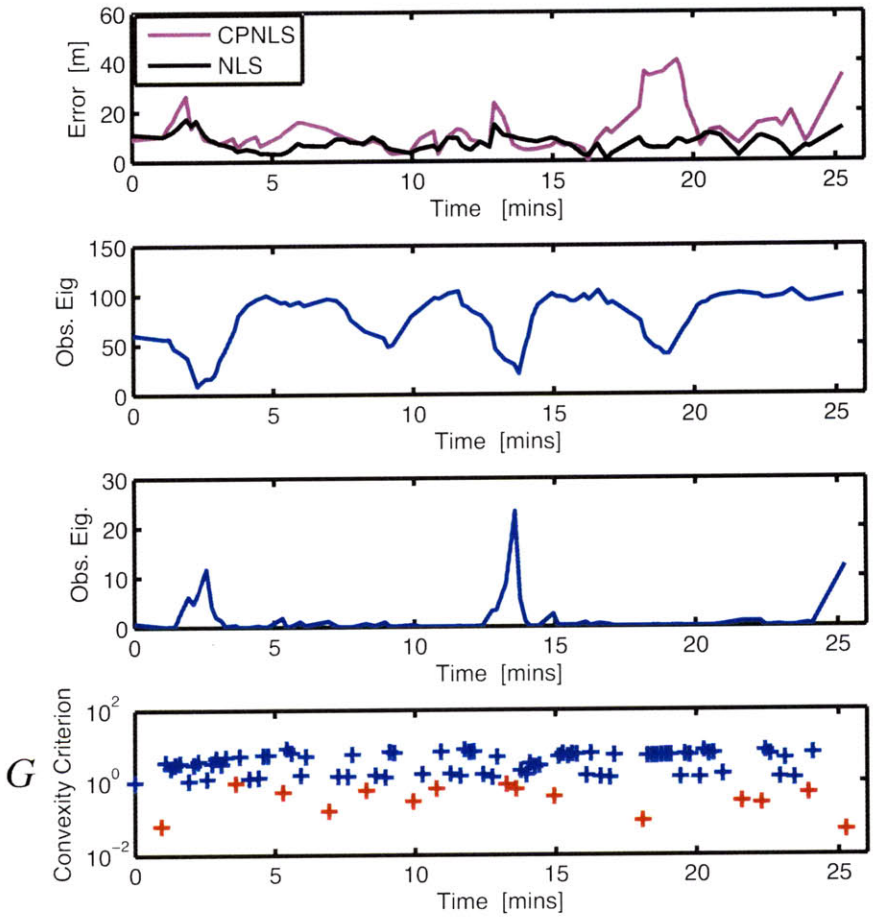

Figure 5-7: The effect of convexity and observability on the localization error for the experiment shown in Figure 5-6.

5.2.3 Experimental Results Using a Kayak and an OceanServer Iver2 AUV

In a second fully realistic experiment, the OceanServer Iver2 AUV carried out a predefined lawnmower pattern running at a depth of 2.4m, while the SCOUT kayak operated as the CNA vehicle by periodically transmitting its GPS position to the AUV via the WHOI modem. Operating the MLBL EKF algorithm entirely online, the OceanServer Iver2 AUV transmitted its own position estimates to the ASV. The ASV then used the estimate to plan locations from which to transmit. Figure 5-8 illustrates the path taken by the underwater vehicle. The test lasted 9 minutes and in total the AUV traveled approximately 500 meters. The AUV surfaced at the end of the experiment and received a GPS fix at (-202, -242), as shown with a red cross in Figure 5-8. At that time the vehicle's onboard filter (green line and green cross) estimated its position to be (-258,-276), while the NLS cooperative localization filter (black line and black cross) produced an estimated position of (-205,-235) and the EKF cooperative localization filter (blue cross) estimated a position of (-260 -253). Our results demonstrate that by using a surface vehicle aiding an AUV, the localization error is reduced. In addition, we have shown that the NLS algorithm outperforms the EKF for localization.

5.3 Summary

This chapter has presented the experimental implementation of cooperative localization using three estimators — the EKF, particle filtering, and NLS. Results were presented for two different experiments, demonstrating the viability of the cooperative ASV/AUV localization concept.

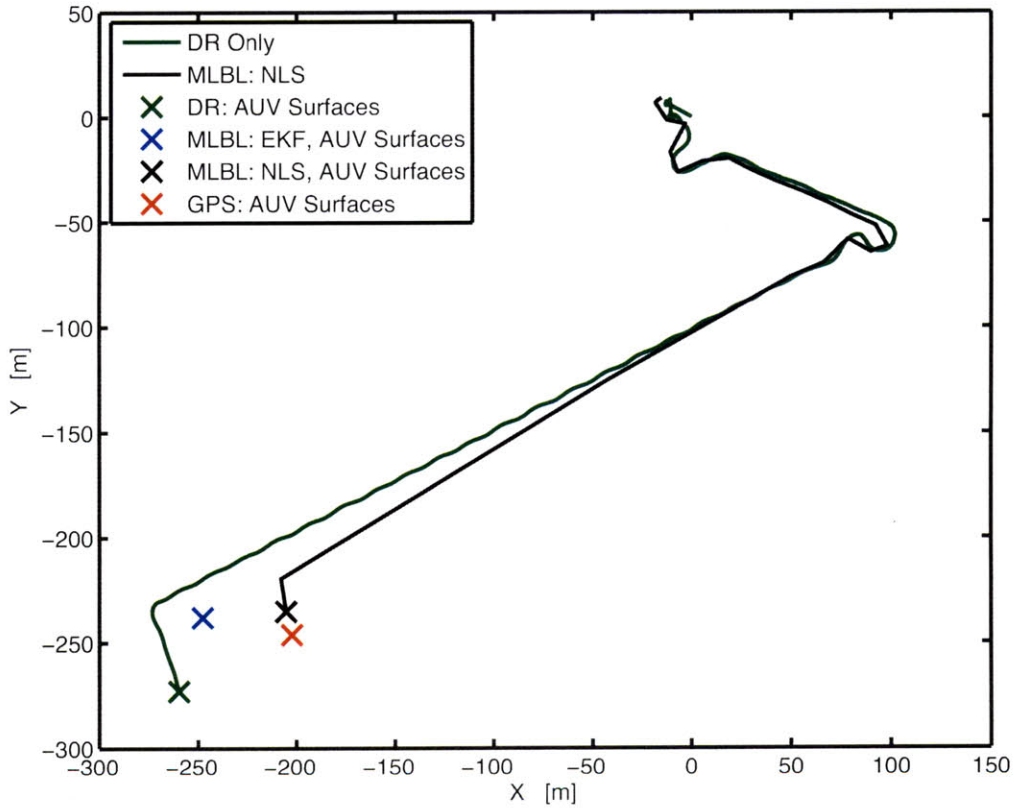

Figure 5-8: MLBL using an OceanServer Iver2 AUV.

THIS PAGE INTENTIONALLY LEFT BLANK

Chapter 6

Conclusions and Future Work

6.1 Contributions

In this work, we studied the cooperative ASV/AUV localization problem assuming inexpensive sensors. This work was a continuation of previous work that utilized two surface vehicles to aid a submerged AUV. In our work, we took the next logical step of using only one surface vehicle, which makes the state estimation much more challenging, due to the issues of observability and convergence. Using the weak observability theorem for non-linear systems, we have shown that the ASV/AUV cooperative localization problem is best addressed using a non-linear observer.

Though we show that the localization problem is non-convex, we have proposed an algorithm that under certain assumptions achieves convergence by choosing initial conditions that lie in convex areas. Our algorithm recursively optimizes the AUV's path for each new dead-reckoning and range pair, using the NLS solution from the previous iteration, subject to a convergence criterion that depends on the relationship between the accuracy of the proprioceptive on-board sensors and the exteroceptive ranging sensor. We have demonstrated the performance of the approach with real data for experiments with one AUV and one autonomous surface craft. We also compare our approach to alternative state estimators, demonstrating superior performance.

6.2 Future Work

One potential alternative for future work is to reparameterize the cooperative localization framework in an alternative linear coordinate space, thus simplifying the required state estimation [9]. In the absence of such a reformulation, nonlinear optimization methods present the state of the art for this problem. Since it is infeasible to operate a typical NLS optimization indefinitely, as the number of states continually increases, future work will consider methods for on-line incremental optimization [23], followed by a full offline batch optimization after the mission.

Another potential idea for future work is to consider the localization problem for a group of AUVs that share information with each other and exchange relative range measurements. In this case, the problem becomes more challenging due to the correlation of the vehicles' positions with each other. For this case, a useful strategy will be to exchange range measurements between all the vehicles and try to keep the rate that the covariance increases bounded and small. Assuming that some of the vehicles are equipped with expensive DVLs, then the position covariance for these vehicles will grow slowly. In the case that the covariance of all the vehicles becomes large, then one one or more vehicles can go to the surface to receive GPS fixes, thereby minimizing their covariances and at the same time providing the other vehicles with corrected position information.

An additional problem for future work is to add sensing of the external environment, both above and below the water. Our current and future work is pursuing the objective of cooperative mapping by marine vehicles in Singapore, as part of the CENSAM project of the Singapore MIT Research Alliance. Figures 6-1 and 6-2 show some of the experimental assets (multiple SCOUT kayaks and an IVER2 AUV) that we have available for this effort. Our ultimate goal is to combine new SLAM algorithms with the cooperative localization techniques presented in this thesis, providing a complete solution for autonomous mapping of complex marine environments using multiple autonomous vehicles.

Figure 6-1: Kayaks on a ship ready to go for an experiment.

Figure 6-2: Kayaks and and OceanServer Iver2 navigating in Singapore.

THIS PAGE INTENTIONALLY LEFT BLANK

Appendix A

Heading Variance Assumption

Consider the equation of motions of a vehicle

$$x_t = x_{t-1} + (v\cos(\theta) - w\sin(\theta))\triangle_t \tag{A.1}$$

$$y_t = y_{t-1} + (w\cos(\theta) + v\sin(\theta))\triangle_t \tag{A.2}$$

For simplicity, we move to the continuous domain:

$$V_x = v\cos(\theta) - w\sin(\theta) \tag{A.3}$$

$$V_y = w\cos(\theta) + v\sin(\theta) \tag{A.4}$$

where v and w are the forward and starboard velocities respectively. These velocities are considered to be random variables and can be written as a combination of a deterministic part and a noise part:

$$v = v_m + n_v \tag{A.5}$$

$$w = w_m + n_w \tag{A.6}$$

Adding the continuous system equations gives

$$V_x + V_y = \cos(\theta)[v + w] + \sin(\theta)[v - w] \tag{A.7}$$

We can also assume that the heading is a random variable, which is a combination of a deterministic part and a noise part:

$$\theta = \theta_m + n_\theta \tag{A.8}$$

Consider the Taylor series expansion of $\cos(\theta)$ and $sin(\theta)$ around θ_m

$$\begin{aligned} \cos(\theta) &\approx cos(\theta_m + n_\theta) \approx \cos\theta_m - (\sin\theta_m)n_\theta + o(E^3) && \text{(A.9)} \\ \sin(\theta) &\approx Sin(\theta_m + n_\theta) \approx \sin\theta_m + (\cos\theta_m)n_\theta + o(E^3) && \text{(A.10)} \end{aligned}$$

Substituting θ, v and w into the above equation yields

$$\begin{aligned} V_x + V_y &= \cos(\theta)[v+w] + sin(\theta)[v-w] \\ &= [\cos\theta_m - (sin\theta_m)n_\theta + o(E^3)] * [v_m + w_m + n_v + n_w] \\ &+ [Sin\theta_m + (cos\theta_m)n_\theta + o(E^3)] * [v_m - w_m + n_v - n_w] \end{aligned} \tag{A.11}$$

Some algebraic simplification gives

$$\begin{aligned} V_x + V_y &= \cos(\theta_m) * [v_m + w_m + n_v + n_w + v_m n_\theta - w_m n_\theta + n_\theta n_v - n_\theta n_w] \\ &+ sin(\theta_m) * [v_m - w_m + n_v - n_w - v_m n_\theta - w_m n_\theta - n_\theta n_v - n_\theta n_w] \end{aligned} \tag{A.12}$$

Defining

$$\begin{aligned} f_1 &= [v_m + w_m + n_v + n_w + v_m n_\theta - w_m n_\theta + n_\theta n_v - n_\theta n_w] && \text{(A.13)} \\ f_2 &= [v_m - w_m + n_v - n_w - v_m n_\theta - w_m n_\theta - n_\theta n_v - n_\theta n_w] && \text{(A.14)} \end{aligned}$$

and substituting gives

$$V_x + V_y = cos(\theta_m) * f_1 + Sin(\theta_m) * f_2 + o(E^3) \tag{A.15}$$

Now we consider a different system with the same kinematics. This system has heading variance equal to zero, and noisy velocity inputs in the forward and starboard directions $(\bar{V}, \bar{W})$. For the new system we have:

$$V_{x,\text{new}} + V_{y,\text{new}} = \cos(\theta)[\bar{v} + \bar{w}] + \sin(\theta)[\bar{v} - \bar{w}] \tag{A.16}$$

Since we want the two systems to behave the same way, we set their velocities to be equal:

$$\begin{aligned} V_{x,new} + V_{y,new} &= cos(\theta)[\bar{v} + \bar{w}] + sin(\theta)[\bar{v} - \bar{w}] \equiv & \text{(A.17)} \\ V_x + V_y &= cos(\theta_m) * f_1 + sin(\theta_m) * f_2 + o(E^3) & \text{(A.18)} \end{aligned}$$

One solution to the above equation is given by the solution of the two equations below:

$$\begin{aligned} f_1 &= \bar{v} + \bar{w} & \text{(A.19)} \\ f_2 &= \bar{v} - \bar{w} & \text{(A.20)} \end{aligned}$$

There is only one solution for the system above, given by

$$\begin{aligned} \bar{v} &= (f_1 + f_2)/2 & \text{(A.21)} \\ \bar{w} &= (f_1 - f_2)/2 & \text{(A.22)} \end{aligned}$$

where f_1, f_2 has been computed in the first part of this proof, so

$$\begin{aligned} \bar{v} &= ((f_1 + f_2)/2 = [v_m + w_m + n_v + n_w + v_m n_\theta - w_m n_\theta + n_\theta n_v - n_\theta n_w] \\ &+ [v_m - w_m + n_v - n_w - v_m n_\theta - w_m n_\theta - n_\theta n_v - n_\theta n_w])/2 & \text{(A.23)} \\ \bar{w} &= ((f_1 + f_2)/2 = [v_m + w_m + n_v + n_w + v_m n_\theta - w_m n_\theta + n_\theta n_v - n_\theta n_w] \\ &- [v_m - w_m + n_v - n_w - v_m n_\theta - w_m n_\theta - n_\theta n_v - n_\theta n_w])/2 & \text{(A.24)} \end{aligned}$$

We finally have:

$$\bar{v} = v_m + n_v - w_m n_\theta - n_\theta n_w \tag{A.25}$$

$$\bar{w} = w_m + n_w + v_m n_\theta + n_\theta n_v \tag{A.26}$$

Finally, assuming zero mean sensor noises, we have:

$$Var(\bar{v}) = Var(v) + (w_m)2 * Var(\theta) + Var(\theta) * Var(w) \tag{A.27}$$

$$Var(\bar{w}) = Var(W) + (v_m)2 * Var(\theta) + Var(\theta) * Var(w) \tag{A.28}$$

$$E[v] = v_m \tag{A.29}$$

$$E[w] = w_m \tag{A.30}$$

Bibliography

[1] A. Alcocer, P. Oliveira, and A. Pascoal. Study and implementation of an EKF GIB-Based underwater positioning system. In *IFAC CAMS04*, 2004.

[2] G. Antonelli, F. Arrichiello, S. Chiaverini, and G. Sukhatme. Observability analysis of relative localization for AUVs based on ranging and depth measurements. In *IEEE Intl. Conf. on Robotics and Automation (ICRA)*, May 2010.

[3] Sanjeev Arulampalam, Simon Maskell, Neil Gordon, and Tim Clapp. A tutorial on particle filters for on-line non-linear/non-gaussian Bayesian tracking. *IEEE Transactions on Signal Processing*, 50:174–188, 2001.

[4] A. Bahr. *Cooperative Localization for Autonomous Underwater Vehicles.* PhD thesis, Massachusetts Institute of Technology, Cambridge, MA, USA, Feb 2009.

[5] A. Bahr and J.J. Leonard. Cooperative Localization for Autonomous Underwater Vehicles. In *Intl. Sym. on Experimental Robotics (ISER)*, Rio de Janeiro, Brasil, Jul 2006.

[6] A. Bahr, J.J. Leonard, and M.F. Fallon. Cooperative localization for autonomous underwater vehicles. *Intl. J. of Robotics Research*, 28(6):714–728, 2009.

[7] Y. Bar-Shalom and T. E. Fortmann. *Tracking and Data Association.* Academic Press, 1988.

[8] M.R. Benjamin, J.J. Leonard, H. Schmidt, and P. Newman. An overview of MOOS-IvP and a brief users guide to the IvP helm autonomy software. (CSAIL-2009-028), Jun 2009.

[9] Joseph Djugash, Sanjiv Singh, and Benjamin P. Grocholsky. Modeling Mobile Robot Motion with Polar Representations. In *IEEE/RSJ Intl. Conf. on Intelligent Robots and Systems (IROS)*, Oct 2009.

[10] R. Eustice, L. Whitcomb, H. Singh, and M. Grund. Recent advances in synchronous-clock one-way-travel-time acoustic navigation. In *Proceedings of the IEEE/MTS OCEANS Conference and Exhibition*, pages 1–6, Boston, MA, USA, 2006.

[11] R. M. Eustice, L. L. Whitcomb, H. Singh, and M. Grund. Experimental Results in Synchronous-Clock One-Way-Travel-Time Acoustic Navigation for Autonomous Underwater Vehicles. In *IEEE Intl. Conf. on Robotics and Automation (ICRA)*, pages 4257–4264, Rome, Italy, Apr 2007.

[12] R.M. Eustice, H. Singh, and J.J. Leonard. Exactly sparse delayed-state filters for view-based SLAM. *IEEE Trans. Robotics*, 22(6):1100–1114, Dec 2006.

[13] M.F. Fallon, G. Papadopoulos, and J.J. Leonard. Cooperative AUV navigation using a single surface craft. In *Field and Service Robotics (FSR)*, Jul 2009.

[14] Lee Freitag, Matt Grund, Sandipa Singh, James Partan, Peter Koski, and Keenan Ball. The WHOI micro-modem: An acoustic communications and navigation system for multiple platforms. In *Proceedings of the IEEE/MTS OCEANS Conference and Exhibition*, volume 1, pages 1086–1092, Sep 2005.

[15] Aditya S. Gadre and Daniel J. Stilwell. A Complete Solution to Underwater Navigation in the Presence of Unknown Currents Based on Range Measurements From a Single Location. In *IEEE/RSJ Intl. Conf. on Intelligent Robots and Systems (IROS)*, 2005.

[16] A.S. Gadre. *Observability Analysis in Navigation Systems with an Underwater Vehicle Application.* PhD thesis, Virginia Polytechnic Institute and State University, 2007.

[17] D. B. Heckman and R. C. Abbott. An acoustic navigation technique. In *IEEE Oceans '73*, pages 591–595, 1973.

[18] O. Hegrenas, D. Berglund, and O. Hallingstad. Model-aided inertial navigation for underwater vehicles. In *IEEE Intl. Conf. on Robotics and Automation (ICRA)*, 2008.

[19] O. Hegrenas, K. Gade, O. Hagen, and P. Hagen. Underwater transponder positioning and navigation of autonomous underwater vehicles. In *Proceedings of the IEEE/MTS OCEANS Conference and Exhibition*, 2009.

[20] R Hermann and AJ Krener. Nonlinear Controllability and Observability. *IEEE Transactions on Automatic Control*, pages 728–740, 1977.

[21] M. Hunt, W. Marquet, D. Moller, K. Peal, W. Smith, and R. Spindel. An acoustic navigation system. Technical Report WHOI-74-6, Woods Hole Oceanographic Institution, 1974.

[22] S. J. Julier and J. K. Uhlmann. A New Extension of the Kalman Filter to Nonlinear Systems. In *The Proceedings of AeroSense: The 11th International Symposium on Aerospace/Defense Sensing, Simulation and Controls, Orlando, Florida.* SPIE, 1997. Multi Sensor Fusion, Tracking and Resource Management II.

[23] M. Kaess, A. Ranganathan, and F. Dellaert. iSAM: Incremental smoothing and mapping. *IEEE Trans. Robotics*, 24(6):1365–1378, Dec 2008.

[24] D. B. Kilfoyle and A. B. Baggeroer. The current state-of-the-art in underwater acoustic telemetry. *IEEE J. Ocean Engineering*, 25(1):4–27, 2000.

[25] James C. Kinsey and Louis L. Whitcomb. Model-based nonlinear observers for underwater vehicle navigation: Theory and preliminary experiments. In *IEEE Intl. Conf. on Robotics and Automation (ICRA)*, Apr 2007.

[26] Winfried Lohmiller and Jean-Jacques E. Slotine. Control system design for mechanical systems using contraction theory. *IEEE Trans. on Automatic Control*, 45(5), May 2000.

[27] B. Jalving M. Mandt, K. Gade. Integrating DGPS-USBL positioning measurements with inertial navigation in the HUGIN 3000 AUV. In *Saint Petersburg International Conference on Integrated Navigation Systems*, Russia, May 2001.

[28] Darren K. Maczka, Aditya S. Gadre, and Daniel J. Stilwell. Implementation of a Cooperative Navigation Algorithm on a Platoon of Autonomous Underwater Vehicles. *Oceans 2007*, pages 1–6, 2007.

[29] I. Mahon, S.B. Williams, O. Pizarro, and M. Johnson-Roberson. Efficient view-based SLAM using visual loop closures. *IEEE Trans. Robotics*, 24(5):1002–1014, Oct 2008.

[30] P. H. Milne. *Underwater Acoustic Positioning Systems.* London: E. F. N. Spon, 1983.

[31] Anastasios I. Mourikis and Stergios I. Roumeliotis. Performance analysis of multirobot cooperative localization. *IEEE Trans. Robotics*, 22(4):666–681, 2006.

[32] R. Negenborn. Robot localization and Kalman filters. Master's thesis, Utrecht University, Sept 2003.

[33] Paul Rigby, Oscar Pizarro, and Stefan B. Williams. Towards geo-referenced AUV navigation through fusion of USBL and DVL measurements. In *Proceedings of the IEEE/MTS OCEANS Conference and Exhibition*, Sep 2006.

[34] J.-J. Slotine and W. Li. *Applied Nonlinear Control.* Prentice-Hall, 1991.

[35] S. Thrun, W. Burgard, and D. Fox. *Probabilistic Robotics.* The MIT press, Cambridge, MA, 2005.

[36] J. Vaganay, J.J. Leonard, J.A. Curcio, and J.S. Willcox. Experimental validation of the moving long base line navigation concept. In *Autonomous Underwater Vehicles, 2004 IEEE/OES*, pages 59–65, Jun 2004.

[37] M. Walter, F. Hover, and J. Leonard. SLAM for ship hull inspection using exactly sparse extended information filters. In *IEEE Intl. Conf. on Robotics and Automation (ICRA)*, pages 1463–1470, 2008.

[38] Sarah E. Webster, Ryan M. Eustice, Christopher Murphy, Hanumant Singh, and Louis L. Whitcomb. Toward a platform-independent acoustic communications and navigation system for underwater vehicles. In *Proceedings of the IEEE/MTS OCEANS Conference and Exhibition*, Biloxi, MS, 2009.

[39] Sarah E. Webster, Ryan M. Eustice, Hanumant Singh, and Louis L. Whitcomb. Preliminary deep water results in single-beacon one-way-travel-time acoustic navigation for underwater vehicles. In *IEEE/RSJ Intl. Conf. on Intelligent Robots and Systems (IROS)*, 2009.

[40] L. Whitcomb, D. Yoerger, and H. Singh. Combined Doppler/LBL based navigation of underwater vehicles. In *Proceedings of the International Symposium on Unmanned Untethered Submersible Technology (UUST)*, May 1999.

[41] L. Whitcomb, D. Yoerger, H. Singh, and D. Mindell. Towards precision robotic maneuvering, survey, and manipulation in unstructured undersea environments. In *Proc. of the Intl. Symp. of Robotics Research (ISRR)*, volume 8, pages 45–54, 1998.

[42] N Wiener. *I am Mathematician.* MIT press, 1956.

[43] Ke Zhou and Stergios I. Roumeliotis. Optimal motion strategies for range-only constrained multi-sensor target tracking, 2006.